A homeostatic interferon-lambda response to bacterial microbiota stimulates preemptive antiviral defense within discrete pockets of intestinal epithelium

Authors: Jacob A. Van Winkle[1], Stefan T. Peterson[2], Elizabeth A. Kennedy[2], Michael J. Wheadon[2], Harshad Ingle[2], Chandni Desai[3], Rachel Rodgers[2,4], David A. Constant[1], Austin P. Wright[1], Lena Li[1], Maxim Artyomov[3], Sanghyun Lee[2], Megan T. Baldridge[2,5#], and Timothy J. Nice[1#]

Affiliations:

[1] Department of Molecular Microbiology and Immunology, Oregon Health and Science University, Portland, OR 97239, USA

[2] Division of Infectious Diseases, Department of Medicine, Edison Family Center for Genome Sciences & Systems Biology, Washington University School of Medicine, St. Louis, MO 63110, USA

[3] Division of Immunobiology, Department of Pathology and Immunology, Washington University School of Medicine, St. Louis, MO 63110, USA

[4] Department of Pediatrics, Washington University School of Medicine, St. Louis, MO 63110, USA

[5] Department of Molecular Microbiology, Washington University School of Medicine, St. Louis, MO 63110, USA

[#]Correspondence to: nice@ohsu.edu (T.J.N.), mbaldridge@wustl.edu (M.T.B.)

Abstract

Interferon-lambda (IFN-λ) protects intestinal epithelial cells (IECs) from enteric viruses by inducing expression of antiviral IFN-stimulated genes (ISGs). Here, we find that bacterial microbiota stimulate a homeostatic ISG signature in the intestine of specific pathogen-free mice. This homeostatic ISG expression is restricted to IECs, depends on IEC-intrinsic expression of IFN-λ receptor (*Ifnlr1*), and is associated with IFN-λ production by leukocytes. Strikingly, imaging of these homeostatic ISGs reveals localization to pockets of the epithelium and concentration in mature IECs. Correspondingly, a minority of mature IECs express these ISGs in public single-cell RNA sequencing datasets from mice and humans. Furthermore, the bacterial component, lipopolysaccharide, partially restores localized ISGs in mice lacking bacterial microbiota. Lastly, IECs lacking *Ifnlr1* are hyper-susceptible to initiation of murine rotavirus infection. These observations indicate that bacterial microbiota stimulate ISGs in localized regions of the intestinal epithelium at homeostasis, thereby preemptively activating antiviral defenses in vulnerable IECs to improve host defense against enteric viruses.

34 **Introduction**

35 Interferons (IFNs) are a family of cytokines produced in response to infection that signal
36 IFN receptor-bearing cells to induce transcription of hundreds of interferon-stimulated genes
37 (ISGs). These ISGs perform diverse functions, but many cooperate to induce an antiviral state
38 (Sadler and Williams, 2008; Schoggins and Rice, 2011). There are three types of IFNs: type I
39 IFNs (IFN-αs, IFN-β, others), type II IFN (IFN-γ), and type III IFNs (IFN-λs). These three types are
40 differentiated by receptor usage (type I IFN receptor: *Ifnar1*/*Ifnar2*; type II IFN receptor:
41 *Ifngr1*/*Ifngr2*; type III IFN receptor: *Ifnlr1*/*Il10rb*), but all three receptor complexes signal through
42 Janus-kinase (JAK) and signal transducer and activator of transcription (STAT) factors to
43 stimulate ISG transcription (Ingle et al., 2018; Schneider et al., 2014). Type I and III IFNs are
44 directly stimulated by host detection of microbe-associated molecular patterns (MAMPs) such as
45 viral nucleic acids, and the prominent contribution of these IFN types to antiviral defense is
46 reflected by the breadth of evasion strategies used by diverse viral families to prevent their
47 production or action (Levy and García-Sastre, 2001; Rojas et al., 2021; Taylor and Mossman,
48 2013). The type I IFN receptor is expressed broadly across most cell types, whereas the type III
49 IFN receptor, *Ifnlr1,* is primarily restricted to epithelial cells (Kotenko and Durbin, 2017;
50 Sommereyns et al., 2008). Accordingly, IFN-λ is of particular importance in effective antiviral
51 defense of barrier tissues.

52 Interestingly, previous studies in mice have noted that intestinal epithelial cells (IECs) are
53 hyporesponsive to type I IFN (Lin et al., 2016; Mahlakõiv et al., 2015; Pott et al., 2011; Van Winkle
54 et al., 2020). The responsiveness of IECs to type I IFN appears to be developmentally regulated
55 because the IECs of adult mice exhibit weaker type I responses than IECs of neonatal mice (Lin
56 et al., 2016). Additionally, infection of mice deficient in IFN receptors (*Ifnar1*, *Ifngr1*, *Ifnlr1*; single
57 or double knockouts) with enteric viruses indicates that IFN-λ is the predominant antiviral IFN type
58 that controls viral replication in the gastrointestinal epithelium (Mahlakõiv et al., 2015; Nice et al.,
59 2015; Pott et al., 2011). IECs can robustly respond to IFN-λ with upregulation of canonical antiviral

60 ISGs and increased resistance to infection by enteric viruses, such as rotaviruses and noroviruses
61 (Baldridge et al., 2017; Nice et al., 2015; Pott et al., 2011). Mouse rotavirus (mRV) is a natural
62 pathogen of mice that infects enterocytes located at the tips of villi in the small intestine (Burns et
63 al., 1995). Rotaviruses have developed mechanisms to antagonize the induction of IFN by
64 infected cells, suggesting that evasion of the IFN response is necessary for efficient epithelial
65 infection (Arnold et al., 2013). Indeed, prophylactic administration of IFN-λ significantly reduces
66 the burden of mRV infection, demonstrating its potential for mediating epithelial antiviral immunity
67 to this pathogen (Hernández et al., 2015; Lin et al., 2016; Pott et al., 2011; Van Winkle et al.,
68 2020). However, a protective role of the endogenous IFN-λ response to mRV infection is less
69 clear, perhaps reflecting the success of mRV evasion mechanisms.

70 Epithelial immunity in the gut must be appropriately balanced to protect the intestinal
71 epithelium while preventing loss of barrier integrity and intrusion by microbes that are abundant
72 within the gastrointestinal tract. The bacterial microbiota in the intestine perform critical functions,
73 aiding in host metabolism (Krajmalnik-Brown et al., 2012), providing a competitive environment
74 to defend against pathogens (Kim et al., 2017), and initiating and maintaining host immune
75 function during homeostasis (Honda and Littman, 2016; Rooks and Garrett, 2016). In this complex
76 environment host epithelial and immune cells detect bacteria and viruses using a suite of pattern
77 recognition receptors (PRRs) that sense the presence of MAMPs. Stimulation of PRRs, such as
78 the toll-like receptor (TLR) family, activates antimicrobial and antiviral defenses providing local
79 protection in many tissues (Chu and Mazmanian, 2013; Iwasaki and Medzhitov, 2015; Thompson
80 et al., 2011). TLR-dependent pathways induce production of IFNs, primarily by signaling through
81 TIR-domain-containing adapter-inducing interferon-β (TRIF) and myeloid differentiation primary
82 response 88 (MYD88) adapter proteins (Monroe et al., 2010; Odendall et al., 2017), providing a
83 mechanism by which bacterial MAMPs can initiate IFN responses.

84 Signals from the bacterial microbiota have been shown to elicit a steady-state type I IFN
85 response in systemic tissues and cell types that can prime antiviral immunity by several

86 independent studies (Abt et al., 2012; Bradley et al., 2019; Ganal et al., 2012; Steed et al., 2017;
87 Stefan et al., 2020; Winkler et al., 2020). Additionally, a steady-state ISG signal has been
88 observed in the intestine of uninfected mice (Baldridge et al., 2015; Lin et al., 2016; Stockinger et
89 al., 2014), but this intestinal response remained poorly characterized. Together with the observed
90 hypo-responsiveness of IECs to type I IFN, these findings suggested that bacterial microbiota
91 may stimulate an IFN-λ response in the gut. To explore this interaction, we undertook the present
92 study to assess the role of bacterial microbiota in induction of enteric ISGs at homeostasis using
93 a combination of broad-spectrum antibiotics (ABX) and genetically modified mice.

94 In this study, we uncovered an ISG signature in IECs that was dependent on the presence
95 of bacteria and IFN-λ signaling (hereafter referred to as 'homeostatic ISGs'). This panel of genes
96 was present in WT mice with conventional microbiota and was reduced in WT mice treated with
97 ABX and in mice lacking *Ifnlr1*. We revealed that homeostatic ISG expression is i) restricted to
98 the intestinal epithelium across both the ileum and colon, ii) independent of type I IFN signaling,
99 and iii) associated with IFN-λ transcript expression by epithelium-associated CD45+ leukocytes.
100 Surprisingly, we found that homeostatic ISGs are not expressed uniformly by all IECs; rather,
101 expression is concentrated in localized pockets of IECs and in differentiated IECs relative to crypt-
102 resident progenitors. These patterns of localized ISG expression are corroborated by
103 independently-generated single-cell RNA sequencing data from mouse and human IECs. We also
104 found that ISG expression can be partially rescued by reconstitution of bacterial microbiota or
105 administration of bacterial lipopolysaccharide (LPS) to ABX-treated mice. Finally, we found that
106 this microbiota-stimulated ISG signature provides protection from initiation of mRV infection.
107 Cumulatively, this study found that bacteria initiate preemptive IFN-λ signaling in localized areas
108 to protect IECs from enteric viruses.

Results

Bacterial microbiota stimulate IFN-λ response genes in the ileum at homeostasis

To determine the effect of bacterial microbiota on homeostatic IFN-λ responses, we compared gene expression in whole ileum tissue for the following experimental groups: i) wild-type C57BL/6J (WT) mice intraperitoneally-injected with IFN-λ as compared to unstimulated WT mice, ii) WT mice with conventional microbiota as compared to WT mice treated with an antibiotic cocktail (ABX) to deplete bacteria, iii) WT mice with conventional microbiota as compared to *Ifnlr1*$^{-/-}$ mice with conventional microbiota, and iv) *Ifnlr1*$^{-/-}$ mice with conventional microbiota compared to *Ifnlr1*$^{-/-}$ mice treated with ABX (**Figure 1A**). To rule out contributions of *Ifnlr1* toward an altered intestinal bacterial microbiota, we performed 16S rRNA sequencing on stool from *Ifnlr1*$^{+/+}$, *Ifnlr1*$^{+/-}$, and *Ifnlr1*$^{-/-}$ mice and did not find differences in alpha-diversity and beta-diversity measurements (**Figure S1**). For each comparison of ileum gene expression shown in **Figure 1A,** we performed gene-set-enrichment-analysis (GSEA) to determine enrichment or depletion of hallmark gene sets (Liberzon et al., 2016). The hallmark gene set that was most enriched in IFN-λ-treated WT mice compared to unstimulated WT mice was INTERFERON_ALPHA_RESPONSE (**Figures S2, 1B**). Therefore, this gene set reflects differences in IFN-λ responses between experimental conditions.

To deplete bacterial microbiota, we administered a cocktail of broad-spectrum antibiotics, and demonstrated that this treatment reduced bacterial 16S gene copies in stool to below the limit of detection (**Figure S3)**. GSEA of WT mice treated with ABX showed a significant depletion (negative enrichment score) of INTERFERON_ALPHA_RESPONSE hallmark genes in the ileum relative to WT mice with conventional microbiota (**Figure 1C**). These data indicate that ISGs are present at steady-state in the ileum of specific-pathogen-free mice with conventional microbiota and suggest that microbiota stimulate expression of these genes in the ileum at homeostasis.

Type I, II, and III IFN responses have substantial gene expression overlap; therefore, to prove that the IFN-λ receptor was necessary for expression of ISGs at homeostasis, we analyzed gene expression in the ileum of *Ifnlr1*$^{-/-}$ mice. Indeed, GSEA showed significant reduction of

135 INTERFERON_ALPHA_RESPONSE hallmark genes in the ileum of *Ifnlr1*$^{-/-}$ mice compared to WT
136 mice (**Figure 1D**). Furthermore, expression of INTERFERON_ALPHA_RESPONSE hallmark
137 genes was not significantly decreased in *Ifnlr1*$^{-/-}$ mice treated with ABX compared to *Ifnlr1*$^{-/-}$ mice
138 with conventional microbiota (**Figure 1E**). In contrast to INTERFERON_ALPHA_RESPONSE,
139 other hallmark gene sets such as INFLAMMATORY_RESPONSE and
140 IL6_JAK_STAT3_SIGNALING were significantly decreased by ABX treatment in both WT mice
141 and *Ifnlr1*$^{-/-}$ mice (**Figure S2**), which indicates a selective requirement for *Ifnlr1* to elicit ISGs and
142 a minimal effect of *Ifnlr1*-deficiency on other microbiota-dependent genes. Together, these
143 findings suggest that *Ifnlr1* is necessary for the bacterial microbiota-dependent expression of ISGs
144 in the ileum at homeostasis. Since ISGs are enriched in mice upon IFN-λ stimulation and are
145 decreased in *Ifnlr1*$^{-/-}$ and ABX-treated mice, we conclude that the bacterial microbiota stimulates
146 IFN-λ responses in the ileum at homeostasis.

147 To define a core set of bacterial microbiota-dependent, *Ifnlr1*-dependent 'homeostatic
148 ISGs', we determined the overlap of differentially expressed genes (DEGs) by defining genes
149 with: i) increased expression upon IFN-λ stimulation in WT mice, ii) decreased expression upon
150 ABX treatment in WT mice, and iii) decreased expression in *Ifnlr1*$^{-/-}$ mice relative to WT mice. The
151 DEGs shared by each of these comparisons comprised a set of 21 genes that are decreased
152 upon treatment with ABX and loss of *Ifnlr1*, and are induced in response to IFN-λ (**Figure 1F**).
153 This set of homeostatic ISGs includes antiviral genes that are dependent on bacterial microbiota
154 and the IFN-λ pathway. Comparison of homeostatic ISG transcript counts between experimental
155 treatments revealed similar insights as prior GSEA analysis. WT mice treated with IFN-λ had
156 higher expression of all homeostatic ISGs than untreated mice, whereas WT mice with a
157 conventional microbiota had higher expression of homeostatic ISGs than *Ifnlr1*$^{-/-}$ mice and ABX-
158 treated mice of both genotypes (**Figure 1G**). We did not detect additional decreases in these
159 homeostatic ISGs in ABX-treated *Ifnlr1*$^{-/-}$ mice relative to conventional *Ifnlr1*$^{-/-}$ mice, suggesting
160 that *Ifnlr1* is necessary for expression of homeostatic ISGs (**Figure 1G**). These results indicate

161 that there is modest but significant expression of ISGs at homeostasis that is lost with *Ifnlr1*
162 deficiency or ABX treatment. Together, these analyses revealed a homeostatic signature of ISGs
163 in the ileum that depends upon the presence of bacterial microbiota and on intact IFN-λ signaling.

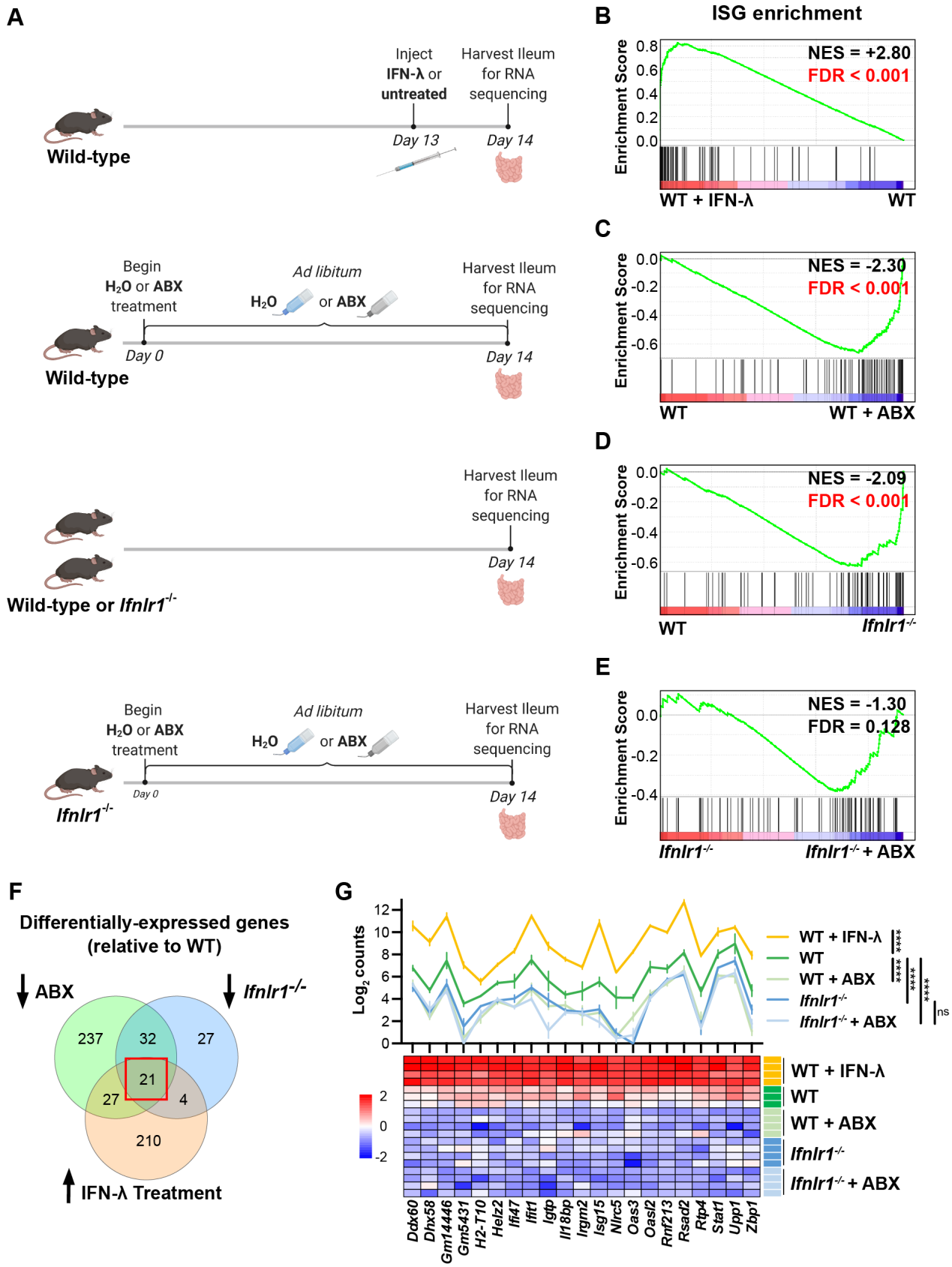
A
Inject IFN-λ or untreated
Harvest Ileum for RNA sequencing
Day 13
Day 14
Wild-type
Begin H2O or ABX treatment
Ad libitum
H2O
or ABX
Harvest Ileum for RNA sequencing
Day 0
Day 14
Wild-type
Harvest Ileum for RNA sequencing
Day 14
Wild-type or Ifnlr1-/-
Begin H2O or ABX treatment
Ad libitum
H2O
or ABX
Harvest Ileum for RNA sequencing
Day 0
Day 14
Ifnlr1-/-
B
ISG enrichment
Enrichment Score
NES = +2.80
FDR < 0.001
WT + IFN-λ
WT
C
Enrichment Score
NES = -2.30
FDR < 0.001
WT
WT + ABX
D
Enrichment Score
NES = -2.09
FDR < 0.001
WT
Ifnlr1-/-
E
Enrichment Score
NES = -1.30
FDR = 0.128
Ifnlr1-/-
Ifnlr1-/- + ABX
F
Differentially-expressed genes (relative to WT)
ABX
Ifnlr1-/-
237
32
27
21
27
4
210
IFN-λ Treatment
G
Log2 counts
WT + IFN-λ
WT
WT + ABX
Ifnlr1-/-
Ifnlr1-/- + ABX
****
****
****
****
****
ns
Ddx60
Dhx58
Gm14446
Gm5431
H2-T10
Helz2
Ifi47
Ifit1
Igtp
Il18bp
Irgm2
Isg15
Nlrc5
Oas3
Oasl2
Rnf213
Rsad2
Rtp4
Stat1
Upp1
Zbp1

165 **Figure 1. Bacterial microbiota stimulate IFN-λ response genes in the ileum at homeostasis.**
166 **A.** Depiction of experimental treatments and comparison groups. Following the indicated
167 treatments, a segment of whole ileum tissue was harvested and analyzed by RNA sequencing for
168 differentially expressed genes between paired conditions. **B-E.** Gene-set enrichment analysis of
169 INTERFERON_ALPHA_RESPONSE hallmark genes (ISGs) was performed with the following
170 comparisons: WT mice treated with 25μg of IFN-λ relative to WT mice treated with PBS **(B)**, WT
171 mice treated with ABX relative to untreated WT mice **(C)**, *Ifnlr1*$^{-/-}$ mice relative to WT mice **(D)**,
172 and *Ifnlr1*$^{-/-}$ mice treated with ABX relative to untreated *Ifnlr1*$^{-/-}$ mice **(E)**. Normalized enrichment
173 score (NES) and false-discovery rate (FDR) are overlaid for each comparison with significant
174 FDR's highlighted (red). **F.** A Venn diagram depicting the total number of differentially expressed
175 genes that are i) increased with IFN-λ stimulation (orange), ii) decreased with ABX treatment
176 (green), or iii) decreased in *Ifnlr1*$^{-/-}$ mice relative to WT (blue). An overlapping subset of 21 genes
177 was shared among all three comparisons (red box). **G.** A graph and heatmap of the relative
178 expression of the 21 genes that overlap in all experimental groups in **F** ('homeostatic ISGs').
179 Statistical significance in **(G)** was determined by one-way ANOVA with Tukey's multiple
180 comparisons where ns = $p > 0.05$, and **** = $p < 0.0001$.

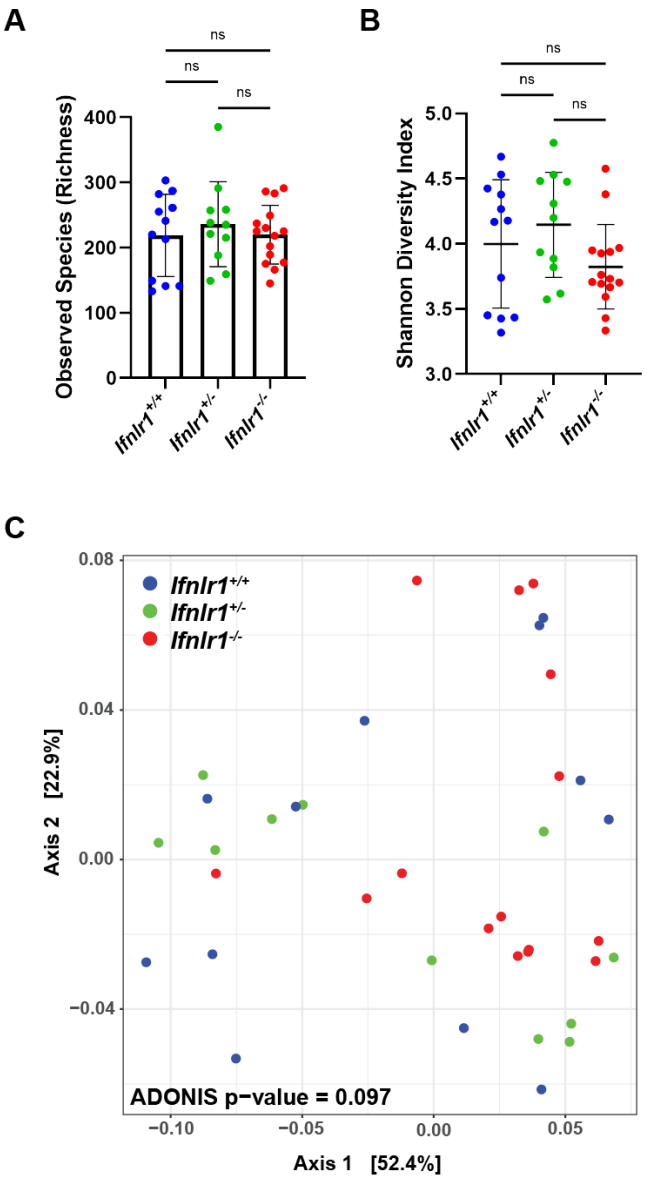

181

182 **Figure S1. *Ifnlr1*-deficiency does not alter intestinal bacterial microbiota.** Stool was
183 harvested from *Ifnlr1*$^{+/+}$, *Ifnlr1*$^{+/-}$, and *Ifnlr1*$^{-/-}$ mice and 16S rRNA genes were sequenced. Alpha-
184 diversity metrics of observed bacterial species (**A**) and Shannon Diversity Index (**B**). **C.** Principle
185 component analysis of beta-diversity UniFrac distances. Statistical significance was determined
186 one-way ANOVA with Tukey's multiple comparisons, where ns = $p > 0.05$.

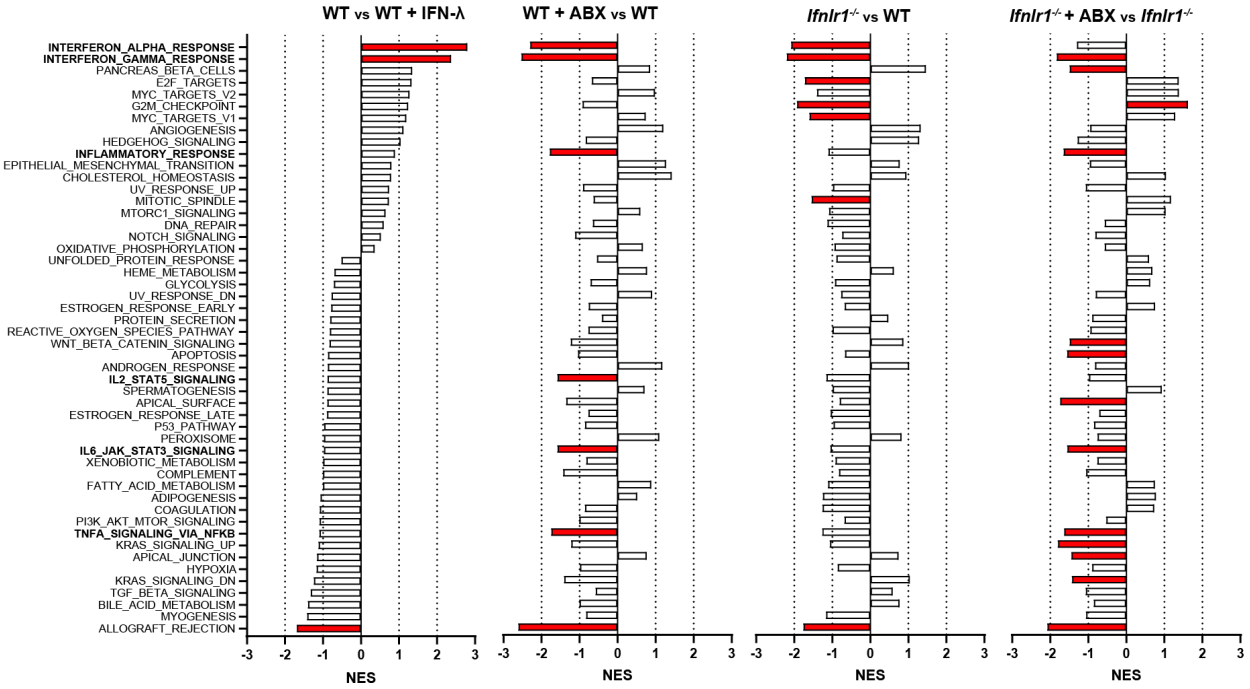

Figure S2. Gene set enrichment analysis of hallmark gene sets. Log_2 counts from RNA sequencing output were assessed for enrichment and depletion of hallmark gene sets by gene set enrichment analysis. Graphs of normalized enrichment score (NES) are displayed for each hallmark gene set and each comparison. Gene sets in red are statistically significantly altered in their given comparison.

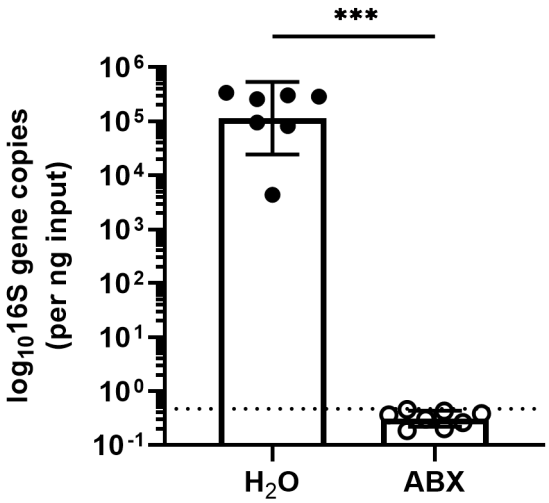

194 **Figure S3. Treatment with antibiotics reduces enteric 16S gene copies to below the limit of**
195 **detection.** rDNA was isolated from luminal contents of mice after 14 days of ABX-treatment. 16S
196 gene copies were assessed by qPCR and normalized to input. Limit of detection: dashed line.
197 Data points represent individual mice and are pooled from 2 independent experiments. Statistical
198 significance was determined by Mann Whitney, where *** = $p < 0.001$.
199

200 **Homeostatic, microbiota- and *Ifnlr1*-dependent ISGs are primarily expressed in intestinal**
201 **tissues**

202 To complement the results of the RNA-sequencing and extend this analysis to other tissue
203 sites**,** we quantified tissue-level expression of a panel of three ISGs by qPCR: *Ifit1, Oas1a*, and
204 *Stat1*. *Ifit1* and *Stat1* were present among the 21 homeostatic ISGs in the preceding analysis and
205 *Oas1a* was included as a representative canonical ISG that we hypothesized would be present in
206 the homeostatic signature, but did not meet the statistical criteria used to define the core set of
207 21 homeostatic ISGs (**Figure 1F and 1G**). We assessed absolute abundance of these ISG
208 transcripts in the ileum, colon, mesenteric lymph nodes (MLN), and spleen of WT and *Ifnlr1*$^{-/-}$ mice
209 with or without ABX treatment (**Figures 2A-C**). Consistent with our RNA-seq data, these ISGs
210 were reduced in the ilea of *Ifnlr1*$^{-/-}$ mice and ABX-treated WT mice compared to WT mice with
211 conventional microbiota (**Figure 2A**). Secondly, homeostatic ISGs were expressed in WT colonic
212 tissue and were significantly decreased in colonic tissue of *Ifnlr1*$^{-/-}$ mice and ABX-treated WT mice
213 (**Figure 2B**). These data indicate that homeostatic ISGs in both the ileum and colon were
214 dependent on *Ifnlr1* and the bacterial microbiota; however, these homeostatic ISGs were more
215 abundantly expressed in ileal tissue than colonic tissue (**Figure S4**). To confirm that treatment
216 with ABX does not ablate the ability of the intestine to respond to IFN-λ, we stimulated WT and
217 ABX-treated mice with intraperitoneal IFN-λ and harvested ileum tissue. Stimulation with small
218 amounts of IFN-λ rescued ISG expression in whole tissue (**Figure S5**), indicating that that

219 reduction of homeostatic ISG expression upon treatment with ABX is not due to an inability of the
220 intestine to respond to IFN-λ.

221 Enteric colonization by bacteria was shown to stimulate systemic type I IFN responses
222 (Abt et al., 2012; Bradley et al., 2019; Ganal et al., 2012; Steed et al., 2017; Stefan et al., 2020;
223 Winkler et al., 2020), so we assessed whether the decreases in ISGs upon ABX treatment or loss
224 of *Ifnlr1* in the ileum were recapitulated in systemic immune tissues. We quantified *Ifit1*, *Stat1,*
225 and *Oas1a* expression in the mesenteric lymph nodes (MLN) spleen and found that ABX
226 treatment and *Ifnlr1* deletion did not reduce ISGs in these tissues (**Figure 2C**). Although we
227 observe increases in *Ifit1* expression in MLN upon treatment with ABX, these results are not
228 recapitulated by *Stat1* and *Oas1a* expression, and no significant changes in ISG expression were
229 detected in the spleen. Cumulatively, these data indicate that homeostatic ISGs include genes
230 beyond the core signature identified in **Figure 1** (e.g. *Oas1a*), that homeostatic ISGs are present
231 in colonic tissue, and that homeostatic IFN-λ stimulated genes are most prominent in enteric
232 tissues.

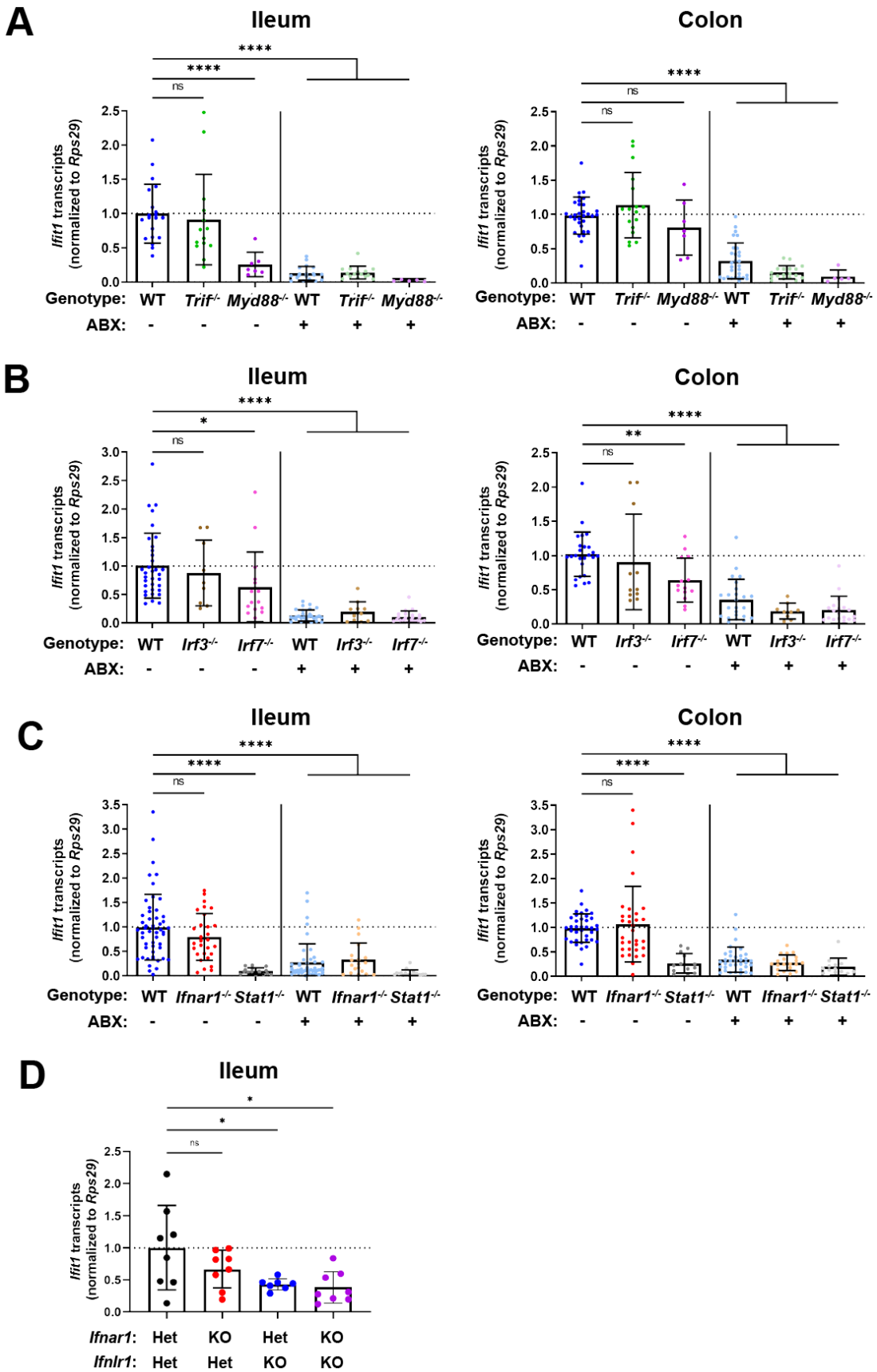
A
Ileum
Colon
Ifit1 transcripts (normalized to Rps29)
Genotype: WT Trif-/- Myd88-/- WT Trif-/- Myd88-/-
ABX: - - - + + +
B
Ileum
Colon
Genotype: WT Irf3-/- Irf7-/- WT Irf3-/- Irf7-/-
ABX: - - - + + +
C
Ileum
Colon
Genotype: WT Ifnar1-/- Stat1-/- WT Ifnar1-/- Stat1-/-
ABX: - - - + + +
D
Ileum
Ifnar1: Het KO Het KO
Ifnlr1: Het Het KO KO

233

Figure 2. Homeostatic, microbiota- and *Ifnlr1*-dependent ISGs are primarily expressed in intestinal tissues. A segment of ileum or colon tissue from WT or *Ifnlr1*$^{-/-}$ mice was harvested following H_2O or ABX treatment and the ISGs *Ifit1*, *Stat1*, and *Oas1a* were analyzed by qPCR. Transcripts were quantified in ileum **(A)**, colon **(B),** or MLN and spleen **(C)** with normalization to untreated WT mice. Data points represent individual mice and data are pooled from 10-20 independent experiments in **A-B** and 15 independent experiments in **C**. Statistical significance was determined by one-way ANOVA with Tukey's multiple comparisons in **A-B** and Dunnett's multiple comparisons in **C**. * = p < 0.05, ** = p < 0.01, *** = p < 0.001, **** = p < 0.0001.

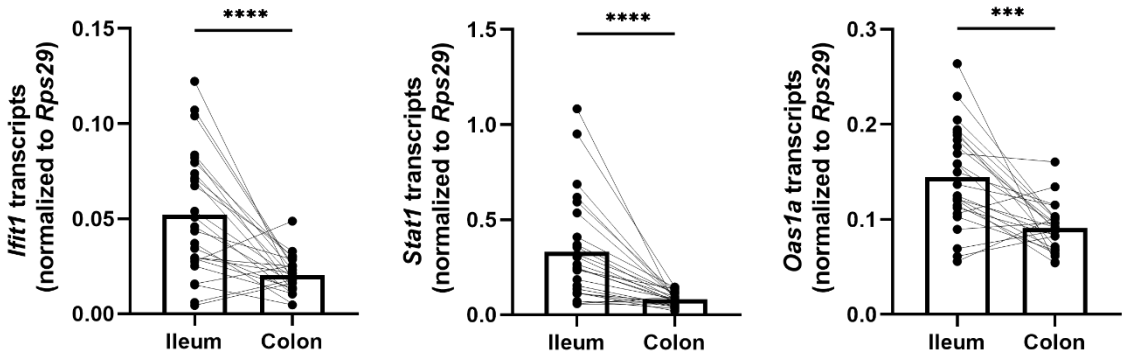

Figure S4. Homeostatic ISGs are more abundantly expressed in the ileum than in the colon. *Ifit1*, *Stat1*, and *Oas1a* expression was quantified from the ileum and colon tissue of WT mice. Data points represent individual mice and are pooled from 5 independent experiments. Statistical significance was determined by paired t-test where *** = p < 0.001 and **** = p < 0.0001.

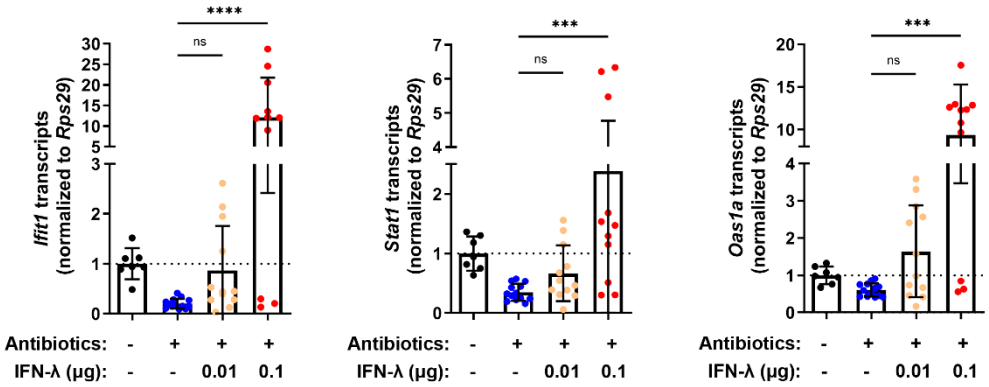

248 **Figure S5. Treatment with antibiotics does not ablate responsiveness to IFN-λ.** *Ifit1*, *Stat1*,
249 and *Oas1a* expression was quantified in the ileum of WT mice treated with or without ABX and
250 was normalized to untreated mice. Increasing quantities of IFN-λ were intraperitoneally injected
251 into ABX-treated mice to rescue basal ISG expression. Data points represent individual mice and
252 are pooled from 3 independent experiments. Statistical significance was determined by Kruskal-
253 Wallis test with Dunn's multiple comparisons with *** = $p < 0.001$, and **** = $p < 0.0001$.
254

255 **Homeostatic ISG expression in the intestine is independent of type I IFN**

256 To determine whether detection of enteric bacteria by TLRs stimulates homeostatic ISGs,
257 we measured tissue ISG expression in mice that were deficient in TRIF or MYD88. Signaling
258 through TRIF results in activation of interferon regulatory factors (IRFs), such as IRF3 and IRF7,
259 that commonly contribute to IFN induction (Honda et al., 2005a; Osterlund et al., 2007; Schmid et
260 al., 2010). Additionally, signaling through MYD88 can aid initiation of IFN expression, through
261 nuclear factor kappa-light-chain-enhancer of activated B cells (NF-κB) transcription factor family
262 members (Osterlund et al., 2007) and IRF7 (Honda et al., 2005b; Tomasello et al., 2018). *Ifit1*
263 expression in the ileum and colon of *Trif*$^{-/-}$ mice was not significantly different than in WT mice,
264 and *Ifit1* expression was reduced with ABX in *Trif*$^{-/-}$ mice (**Figure 3A**). However, we found that
265 mice lacking *Myd88* exhibited tissue-specific decreases in *Ifit1* expression, with significant
266 decreases in the ileum, but not in the colon, relative to WT mice (**Figure 3A)**. These data are
267 consistent with a previous report (Stockinger et al., 2014) and suggest that signaling through
268 MYD88, but not TRIF, is necessary for homeostatic ISG expression in the ileum, whereas other
269 factors may dominate in the colon.

270 To expand these findings, we assessed the role of IRF3 and IRF7 transcription factors
271 that are commonly activated downstream of MYD88 and TRIF. We did not observe significant
272 decreases in *Ifit1* expression in the ileum or the colon of *Irf3*$^{-/-}$ mice as compared to WT (**Figure**
273 **3B**), indicating that IRF3 is not required for homeostatic IFN-λ induction. However, we observed

274 a modest (two-fold) decrease in *Ifit1* expression in both the ileum and colon of *Irf7*$^{-/-}$ mice when
275 compared to WT mice (**Figure 3B**). Although IRF7 is implicated by these data, it does not appear
276 to be strictly required for homeostatic expression of *Ifit1* because expression is further reduced
277 by ABX treatment (**Figure 3B**). These data suggest that IRF7 is not necessary for the homeostatic
278 ISG response to the bacterial microbiota.

279 Type I and III IFNs stimulate overlapping ISG responses that are both dependent on
280 STAT1. Therefore, to further investigate the contribution of type I IFN signaling to homeostatic
281 ISG expression, we quantified *Ifit1* expression in ileum and colon tissue from *Ifnar1*$^{-/-}$ or *Stat1*$^{-/-}$
282 mice. *Ifit1* expression was not significantly different in either ileum or colon tissue of *Ifnar1*$^{-/-}$ mice
283 compared to WT (**Figure 3C**). However, *Ifit1* expression was significantly lower in ileum and colon
284 tissue of *Stat1*$^{-/-}$ mice compared to *Ifnar1*$^{-/-}$ and WT mice. Importantly, treatment of *Stat1*$^{-/-}$ mice
285 with ABX did not further reduce *Ifit1* expression, emphasizing the necessity of STAT1 for this
286 homeostatic ISG response.

287 Lastly, to determine whether type I IFN signaling plays a compensatory role in homeostatic
288 ISG expression in the absence of *Ifnlr1*, we bred mice with heterozygous expression of both *Ifnlr1*
289 and *Ifnar1* (*Ifnlr1*^{Het}/*Ifnar1*^{Het}) with mice that lack *Ifnlr1* and *Ifnar1* (*Ifnlr1*^{KO}/*Ifnar1*^{KO}). This breeding
290 scheme produced littermate-matched mice that were *Ifnlr1*^{Het}/*Ifnar1*^{Het}, *Ifnlr1*^{KO}/*Ifnar1*^{KO}, and mice
291 singly deficient in *Ifnlr1* (*Ifnlr1*^{KO}/*Ifnar1*^{Het}) or *Ifnar1* (*Ifnlr1*^{Het}/*Ifnar1*^{KO}). We found that *Ifit1*
292 expression was not significantly different in *Ifnlr1*^{Het}/*Ifnar1*^{KO} relative to *Ifnlr1*^{Het}/*Ifnar1*^{Het} controls
293 in stripped epithelium (**Figure 3D**). *Ifit1* expression in *Ifnlr1*^{KO}/*Ifnar1*^{Het} was significantly lower
294 compared to *Ifnlr1*^{Het}/*Ifnar1*^{Het} controls, but was not significantly different from *Ifnlr1*^{KO}/*Ifnar1*^{KO}
295 mice (**Figure 3D**). Cumulatively, these data indicate that homeostatic ISG expression in the
296 intestine is partly dependent on MYD88, and is independent of type I IFN signaling.

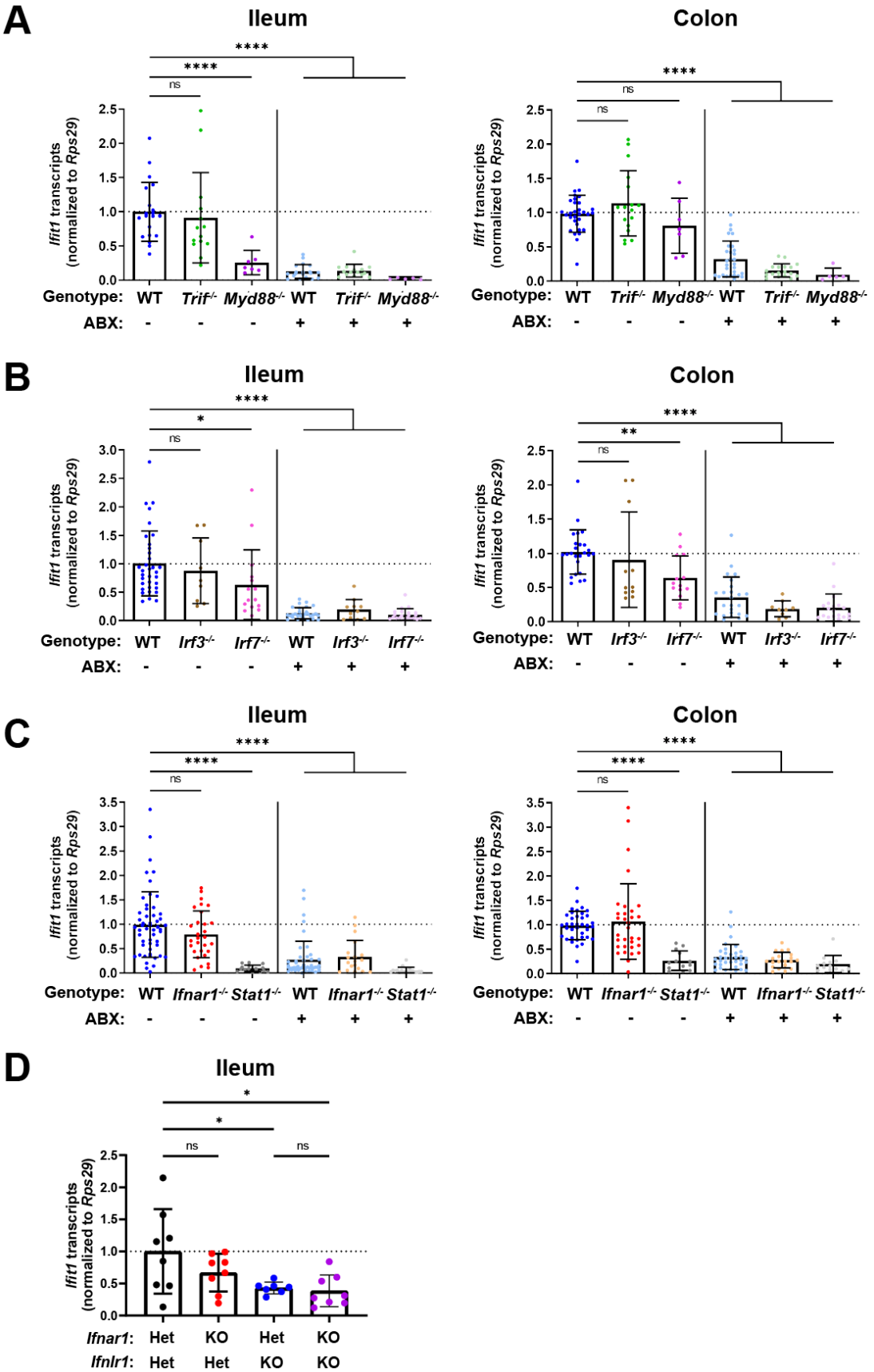
A
Ileum
Colon
Ifit1 transcripts (normalized to Rps29)
Genotype: WT Trif-/- Myd88-/- WT Trif-/- Myd88-/-
ABX: - - - + + +
B
Ileum
Colon
Genotype: WT Irf3-/- Irf7-/- WT Irf3-/- Irf7-/-
ABX: - - - + + +
C
Ileum
Colon
Genotype: WT Ifnar1-/- Stat1-/- WT Ifnar1-/- Stat1-/-
ABX: - - - + + +
D
Ileum
Ifnar1: Het KO Het KO
Ifnlr1: Het Het KO KO

297

298 **Figure 3. Homeostatic ISG expression is independent of type I IFN.** *Ifit1* expression levels
299 were assessed by qPCR from the ileum or colon of **(A)** *Trif*$^{-/-}$ and *Myd88*$^{-/-}$, **(B)** *Irf3*$^{-/-}$ *and Irf7*$^{-/-}$, or
300 **(C)** *Ifnar1*$^{-/-}$ and *Stat1*$^{-/-}$ mice treated with or without ABX normalized to untreated, WT mice. Some
301 WT controls are shared across experiments in **(A-C). D.** *Ifit1* expression was measured by qPCR
302 in ileum tissue of indicated genotypes. Data points represent individual mice and are pooled from
303 at least six independent experiments in **A-C** and two independent experiments in **D**. Statistical
304 significance was determined by one-way ANOVA with Dunnett's multiple comparisons in **A-C** and
305 one-way ANOVA with Tukey's multiple comparisons in D, where * = $p < 0.05$, ** = $p < 0.01$, *** =
306 $p < 0.001$, **** = $p < 0.0001$.
307

308 **Homeostatic ISG expression in the intestine is restricted to epithelial cells**

309 Given the primarily epithelial expression of *Ifnlr1*, we assessed which compartment of the
310 ileum expresses homeostatic ISGs by isolating a stripped intestinal epithelial fraction and digested
311 underlying lamina propria. We assessed ISG expression in these two fractions from WT and *Ifnlr1*$^{-}$
312 $^{/-}$ mice treated with or without ABX. Treatment with ABX or loss of *Ifnlr1* reduced homeostatic
313 ISGs in the IEC fraction, but the lamina propria had low expression of these ISGs relative to the
314 epithelium of untreated WT mice, regardless of treatment or genotype (**Figure 4A**).

315 IECs express abundant *Ifnlr1*, but other intra-epithelial cell types do not (Mahlakõiv et al.,
316 2015; Sommereyns et al., 2008). To determine whether *Ifnlr1* expression by IECs was required
317 for homeostatic ISG expression, we used mice with IECs that are conditionally deficient in *Ifnlr1*
318 (*Ifnlr1*$^{\Delta IEC}$) and littermates that retain normal *Ifnlr1* expression (*Ifnlr1*$^{flox/flox}$) (Baldridge et al., 2017).
319 *Ifit1* and *Oas1a* expression in the ileum (**Figure 4B**) and colon (**Figure 4C**) of *Ifnlr1*$^{flox/flox}$ mice was
320 decreased upon treatment with ABX, consistent with the phenotype observed in WT mice.
321 Conditional deletion of *Ifnlr1* in IECs reduced *Ifit1* and *Oas1a* to a similar extent as the reduction
322 observed in *Ifnlr1*$^{-/-}$ animals, above (**Figures 2A and 2B**). Together, these findings indicate that
323 homeostatic ISGs are dependent on *Ifnlr1*-expression by IECs.

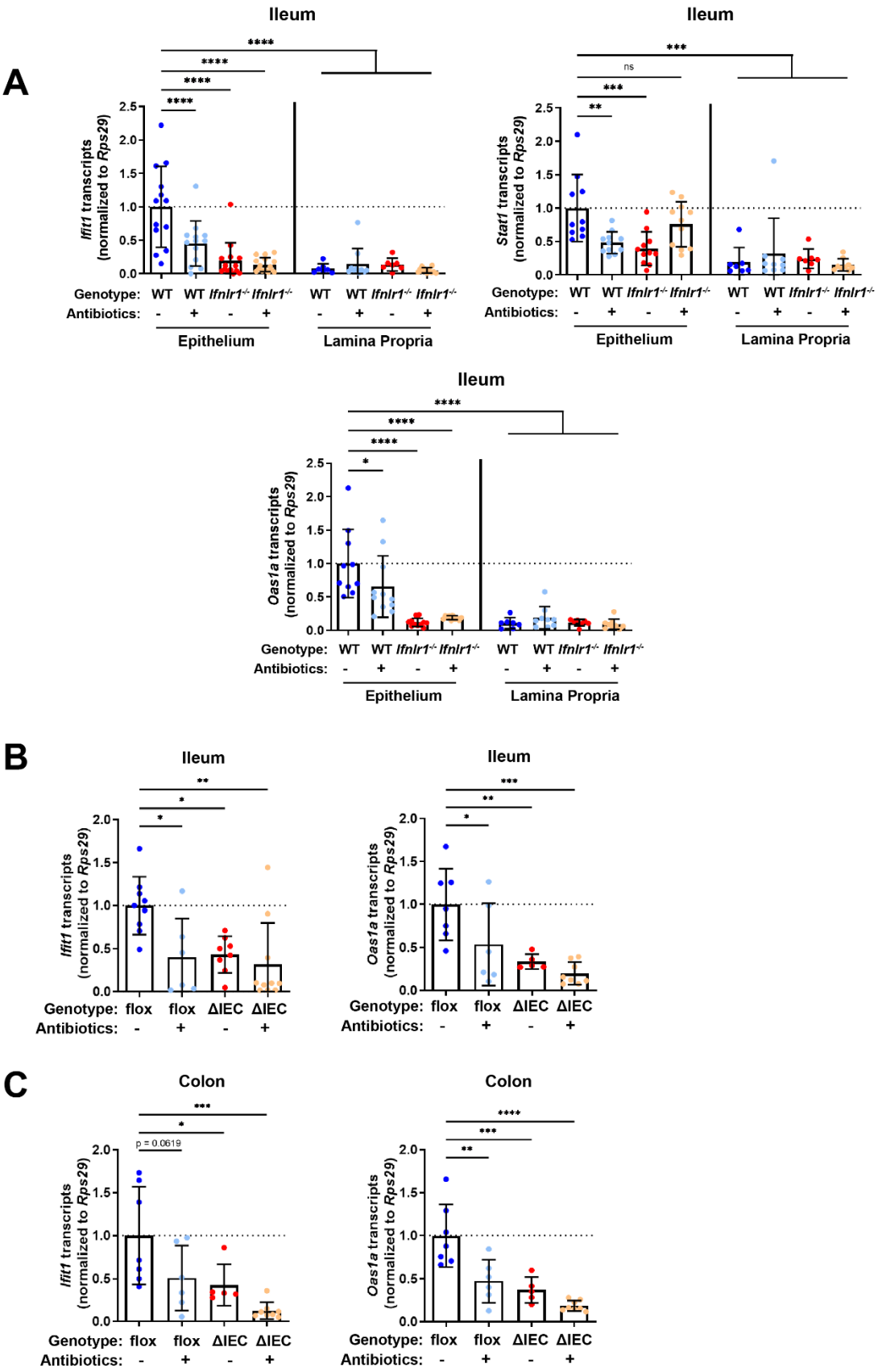
A
Ileum
Ifit1 transcripts (normalized to Rps29)
Genotype: WT WT Ifnlr1-/- Ifnlr1-/- WT WT Ifnlr1-/- Ifnlr1-/-
Antibiotics: - + - + - + - +
Epithelium
Lamina Propria
Ileum
Stat1 transcripts (normalized to Rps29)
ns
Ileum
Oas1a transcripts (normalized to Rps29)
B
Ileum
Ifit1 transcripts (normalized to Rps29)
Genotype: flox flox ΔIEC ΔIEC
Antibiotics: - + - +
Ileum
Oas1a transcripts (normalized to Rps29)
C
Colon
p = 0.0619
Colon

324

325 **Figure 4. Homeostatic ISG expression in the intestine is restricted to epithelial cells**. **A.**
326 *Ifit1*, *Stat1*, and *Oas1a* expression was quantified in stripped epithelial cells or in the lamina
327 propria cells of the ileum. Comparisons were performed between WT and *Ifnlr1*$^{-/-}$ mice with or
328 without ABX treatment, and ISG expression was normalized to WT values. **B and C.** *Ifit1* and
329 *Oas1a* expression from the **(B)** ileum or **(C)** colon of mice with conditional presence (flox) or
330 absence (ΔIEC) of *Ifnlr1* in intestinal epithelial cells. Data points represent individual mice and are
331 pooled from three independent experiments in **A** and two independent experiments in **B-C**.
332 Statistical significance was determined by one-way ANOVA with Dunnett's multiple comparisons.
333 * = $p < 0.05$, ** = $p < 0.01$, *** = $p < 0.001$.
334

335 **Bacterial microbiota stimulate expression of *Ifnl2/3* by CD45-positive cells**

336 A previous study (Mahlakõiv et al., 2015) noted the presence of IFN-λ transcripts (*Ifnl2/3*)
337 at homeostasis in CD45+ cells within the stripped intestinal epithelium, but not in the lamina
338 propria. To extend these findings and to determine whether CD45+ cells in the intestinal
339 epithelium produce IFN-λ in response to bacterial microbiota at homeostasis, we enriched cell
340 subsets from epithelial or lamina propria fractions of the ileum for quantification of *Ifnl2/3* by qPCR.
341 We treated WT mice with control, ABX, or stimulation with a synthetic dsRNA analogue (poly I:C).
342 We then magnet-enriched EpCAM+ or CD45+ cells from stripped intestinal epithelium or digested
343 lamina propria ileal tissue (**Figure S6**). We found that CD45+ cells from the intestinal epithelial
344 and lamina propria fraction expressed detectable *Ifnl2/3* at homeostasis, but EpCAM+ cells did
345 not, which is consistent with Mahlakõiv et al. Furthermore, we found that expression of *Ifnl2/3* in
346 CD45+ cells from the epithelial fraction was significantly reduced with ABX-treatment, and CD45+
347 cells from lamina propria had a non-statistically-significant ($p = 0.0523$) reduction in *Ifnl2/3*
348 expression with ABX-treatment (**Figure 5A**). From these data, we conclude that epithelium-
349 associated CD45+ leukocytes are the likely source of homeostatic IFN-λ in response to bacterial
350 microbiota, but we do not rule out additional involvement of CD45+ cells in the lamina propria.

351 Similar to *Ifnl2/3*, we found that CD45+ cells of the epithelial fraction modestly expressed
352 IFN-β transcript (*Ifnb1*) at homeostasis. Additionally, CD45+ cells of the lamina propria robustly
353 expressed *Ifnb1* at homeostasis. However, unlike *Ifnl2/3*, *Ifnb1* was not decreased in mice treated
354 with ABX (**Figure 5B**). These data indicate that *Ifnb1* expression by CD45+ cells in the intestine
355 is less dependent on stimulation by bacterial microbiota relative to *Ifnl2/3*, consistent with the
356 dominant role of IFN-λ responses in driving homeostatic ISG expression in the epithelium.

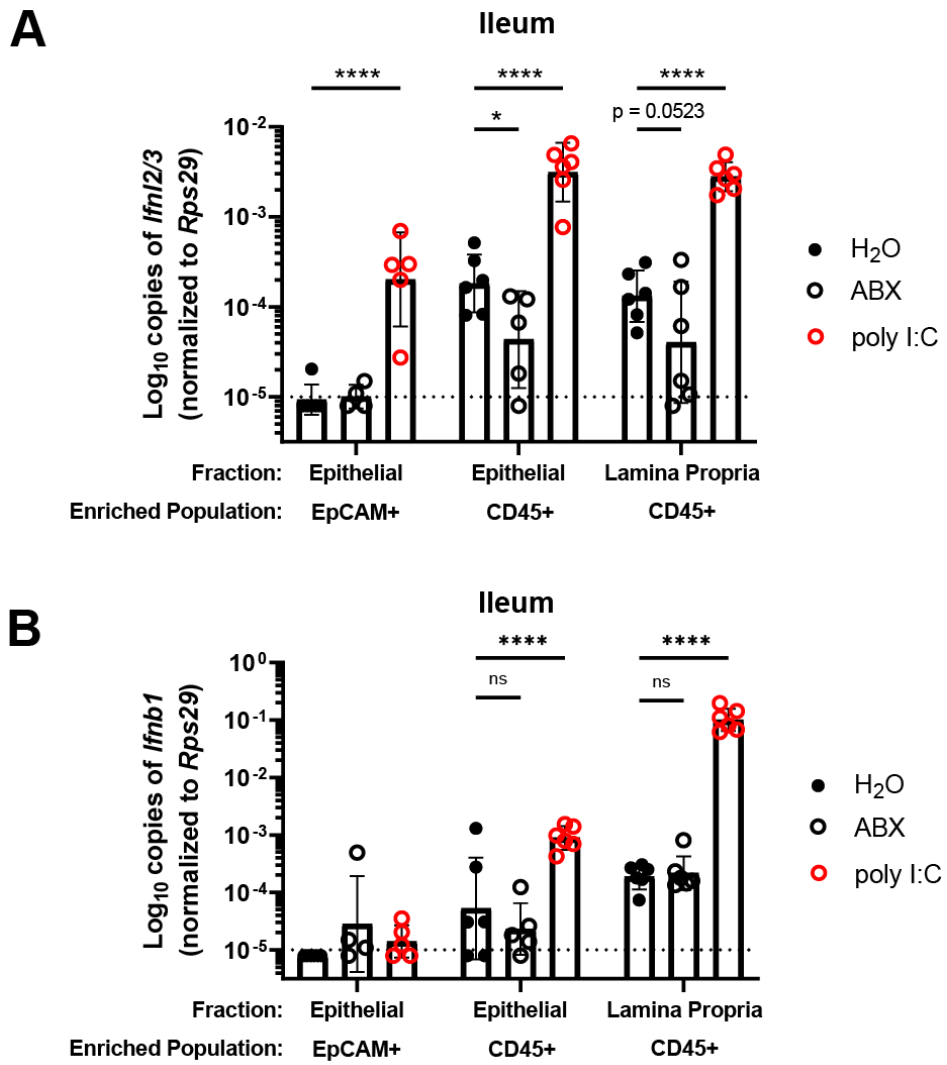

357

358 **Figure 5. Bacterial microbiota stimulate expression of *Ifnl2/3* by CD45-positive cells. A-B.**
359 Cellular suspensions from the ileal epithelium and lamina propria was harvested from WT mice
360 treated with H_2O, ABX, or stimulated with poly I:C. Resulting cells were enriched for EpCAM-

positive and CD45-positive cells by magnetic separation. *Ifnl2/3* expression **(A)** and *Ifnb1* expression **(B)** was quantified from each enriched cellular fraction by qPCR. Data points represent individual mice and are pooled from 2 independent experiments. Statistical significance was determined by two-way ANOVA with Dunnett's multiple comparisons, where * = $p < 0.05$ and **** = $p < 0.0001$.

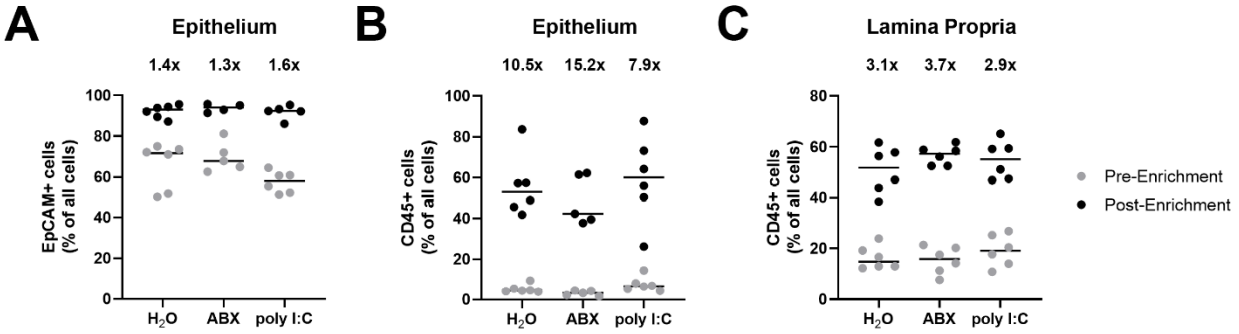

Figure S6. Enrichment of EpCAM+ and CD45+ cells from the intestinal epithelium and lamina propria. A-C. The ileal epithelium and lamina propria was harvested from WT mice treated with H_2O, ABX, or stimulated with poly I:C. Resulting cell suspensions were enriched for EpCAM-positive and CD45-positive cells and the purity of all live and dead cells pre- and post-enrichment were quantified by flow cytometry. The percentage of live and dead cells with surface expression of **(A)** EpCAM or **(B)** CD45 prior to- and following- enrichment from stripped intestinal epithelium. **C.** The percentage of live and dead cells events with surface expression of CD45 prior to and following CD45 enrichment from isolated lamina propria. Mean fold enrichment for each condition is noted above each column. Data points represent individual mice and are pooled from 2 independent experiments.

Homeostatic ISG expression in the small intestine is highly localized

Homeostatic ISG expression in the ileum was of relatively low magnitude when compared to IFN-λ treatment (**Figures 1-2**). Therefore, we hypothesized that a low abundance of homeostatic ISG expression would be uniformly distributed between IECs of the intestinal

382 epithelium, and we sought to assess the distribution of the homeostatic ISG, *Ifit1*, using *in situ*
383 hybridization (RNAscope) (**Figures 6A-G**). Contrary to our hypothesis, RNAscope staining of the
384 ileum from untreated WT mice revealed localized pockets of robust *Ifit1* expression in individual
385 villi rather than ubiquitously low expression throughout the intestinal epithelium (**Figure 6A**).
386 Additionally, *Ifit1* localization was skewed away from the crypt and towards the tips of individual
387 villi within the ileum, and this localization was not specific to *Ifit1* because the distinct ISG *Usp18*
388 co-localized with *Ifit1* (**Figure 6A**). These data indicate that homeostatic ISGs are sporadically
389 expressed in individual villi and are primarily localized to mature enterocytes that are most distally
390 located in villi. We determined that localized ISG expression within individual villi was not due to
391 a localized ability to respond to IFN-λ because stimulation with exogenous IFN-λ resulted in *Ifit1*
392 expression within all intestinal villi, but not intestinal crypts (**Figure S7**). The minimal expression
393 of *Ifit1* within intestinal crypts following exogenous IFN-λ treatment suggests that homeostatic
394 ISGs are localized to mature enterocytes because intestinal crypts do not exhibit robust
395 responses to IFN-λ. Additionally, the non-uniform distribution of homeostatic *Ifit1* expression was
396 ablated in the ileum of mice treated with ABX (**Figures 6B-D**), consistent with a dependency on
397 bacterial microbiota. To determine whether localized *Ifit1* expression was dependent on IEC
398 expression of *Ifnlr1*, we assessed the distribution of *Ifit1* expression in the ilea of littermate
399 *Ifnlr1*$^{flox/flox}$ and *Ifnlr1*$^{\Delta IEC}$ mice. We found that the localized *Ifit1* expression observed in untreated
400 WT mice was recapitulated in *Ifnlr1*$^{flox/flox}$ mice (**Figure 6E**), but these areas of ISG expression
401 were ablated in *Ifnlr1*$^{\Delta IEC}$ mice (**Figures 6F and 6G**). Lastly, we found that this discrete localization
402 of the homeostatic ISG response is not limited to the ileum, as localized *Ifit1* staining is also
403 observed in the colonic epithelium (**Figure S8**). Together, our analyses indicated that homeostatic
404 ISGs are expressed in a highly localized manner within the intestinal epithelium.

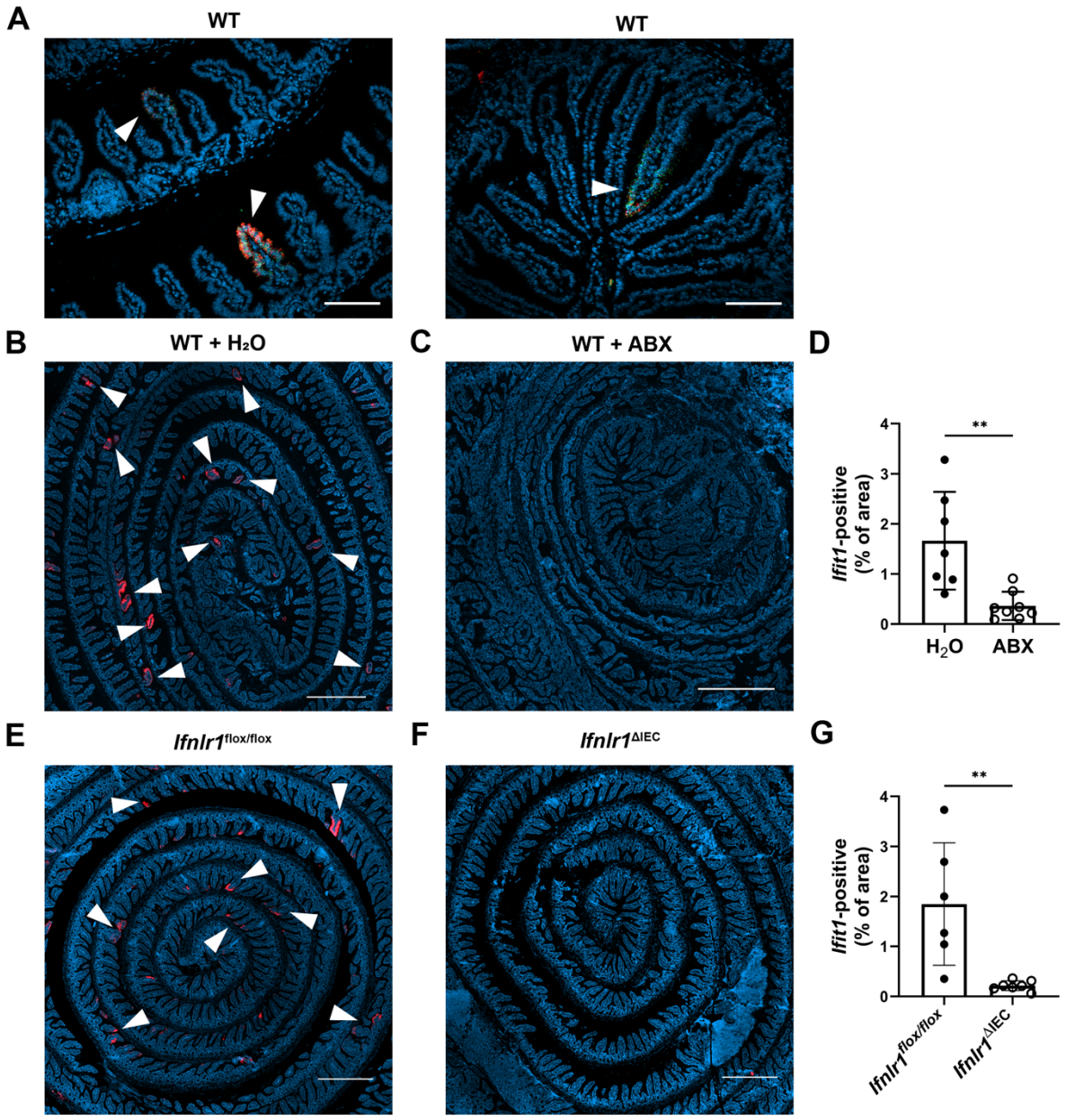

405

406 **Figure 6. Homeostatic ISG expression in the small intestine is highly localized**. The ilea of
407 WT, *Ifnlr1*$^{flox/flox}$, or *Ifnlr1*$^{\Delta IEC}$ mice were harvested, processed into a Swiss rolls, and stained by *in*
408 *situ* hybridization for the ISGs, *Ifit1* (red) and *Usp18* (green), with a DAPI (blue) counterstain. **A.**
409 Representative high-magnification images of co-localized *Ifit1* (red) and *Usp18* (green)
410 expression in the ileum of WT mice, see arrows. **B-D.** WT mice treated with H_2O control or ABX
411 with quantification of *Ifit1* area relative to the total area of the section across replicate mice. **E-G.**
412 *Ifnlr1*$^{flox/flox}$ or *Ifnlr1*$^{\Delta IEC}$ mice at homeostasis with quantification of *Ifit1* area relative to the total area

413 of the section across replicate mice. Scale bar = 100μm in **A** and 500μm in **B-G** and. Statistical
414 significance was calculated by unpaired t-test where ** = p < 0.01. Each data point in **D** and **G**
415 represents an individual mouse from 2 independent experiments.

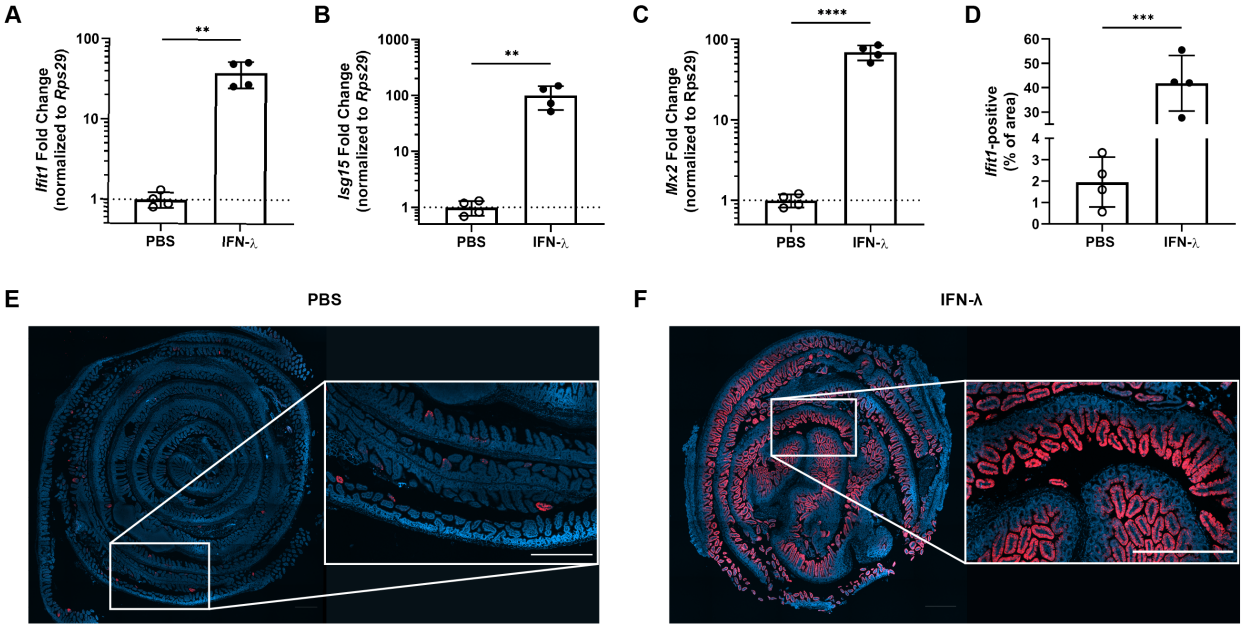

416

417 **Figure S7. The entire intestinal epithelium is responsive to IFN-λ.** Wild-type mice were
418 injected with PBS or 3μg of pegylated IFN-λ3. The ileum was harvested after four hours and a
419 small section was assessed for expression of the ISGs: *Ifit1* **(A)**, *Isg15* **(B)**, and *Mx2* **(C)** by qPCR.
420 The remaining tissue was stained by RNAscope for the ISG, *Ifit1* (red), with a DAPI (blue)
421 counterstain. **D.** Quantification of *Ifit1* area relative to the total area of the section across replicate
422 mice. **E-F.** Representative images from the ileum of mice injected with PBS **(E)** or IFN-λ **(F).**
423 Scale bar = 500μm in insets. Data points represent individual mice from a single experiment.
424 Statistical significance was determined by unpaired t-test with ** = p < 0.01, *** = p < 0.001, and
425 **** = p < 0.0001.

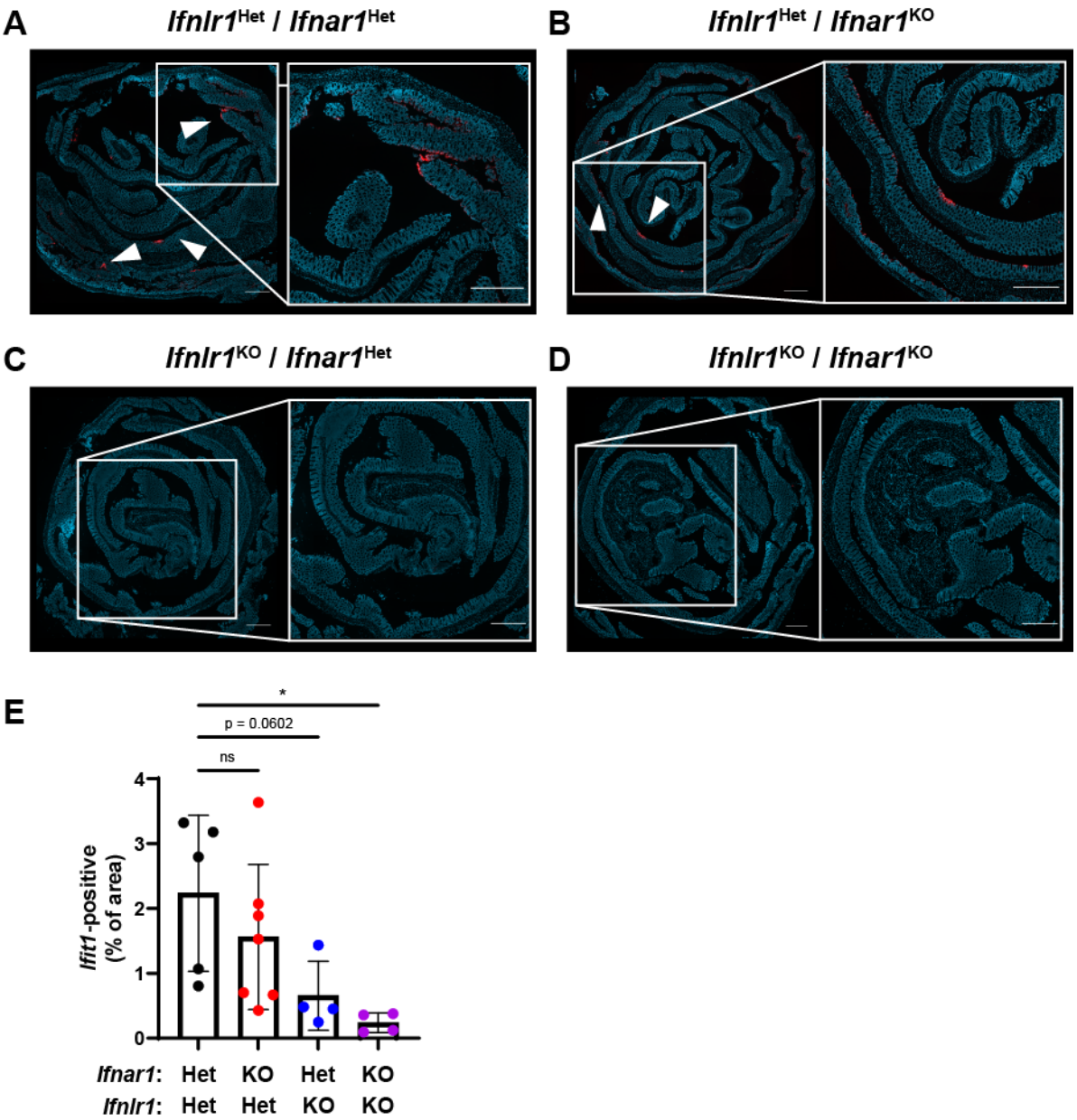

Figure S8. Homeostatic ISG expression is also highly localized in the colon. The colon of *Ifnlr1*^{Het}/*Ifnar1*^{Het}, *Ifnlr1*^{Het}/*Ifnar1*^{KO}, *Ifnlr1*^{KO}/*Ifnar1*^{Het}, and *Ifnlr1*^{KO}/*Ifnar1*^{KO} mice was harvested and stained by RNAscope for the ISG, *Ifit1* (red), with a DAPI (blue) counterstain. Representative images from **(A)** *Ifnlr1*^{Het}/*Ifnar1*^{Het}**,** **(B)** *Ifnlr1*^{Het}/*Ifnar1*^{KO}, **(C)** *Ifnlr1*^{KO}/*Ifnar1*^{Het}, and **(D)** *Ifnlr1*^{KO}/*Ifnar1*^{KO} mice with **(E)** quantification of *Ifit1* area from individual mice. Data are representative of two independent experiments. Scale bar = 500μm.

434 **Mature enterocytes express homeostatic ISGs in public single-cell datasets from mouse**
435 **and human**

436 To determine the extent of conservation of homeostatic ISG expression by IECs, we
437 performed orthogonal analyses of publicly available single-cell RNA-seq (scRNA-seq) datasets
438 from mouse (Haber et al., 2017) and human (Elmentaite et al., 2020) IECs. Recently, Haber et al.
439 published a large single-cell RNA sequencing dataset that profiled sorted IECs from the small
440 intestine of specific-pathogen-free mice and defined 15 distinct IEC subtypes (Haber et al., 2017).
441 We analyzed IECs from this dataset, and found that of the 21 homeostatic ISGs identified in
442 **Figure 1D**, 19 were present in the Haber et al. single-cell dataset. We determined the percentage
443 of each epithelial cell subtype that expresses each individual homeostatic ISG, and generated a
444 heatmap with hierarchical clustering to group IEC subtypes that have similar ISG expression
445 patterns (**Figure 7A**). Homeostatic ISGs were predominantly expressed in mature enterocyte
446 subtypes, which clustered separately from crypt-resident progenitor IECs such as transit
447 amplifying (TA) cells and stem cells (**Figure 7A**). To compare homeostatic ISG expression
448 between polar extremes of the crypt-villus axis, we grouped IEC subtypes that represented
449 enterocytes (mature enterocyte cells) and crypt-associated cells (TA cells and stem cells) to
450 compare the overall proportions of these cells with homeostatic ISG expression. We found that a
451 significantly higher percentage of enterocytes express homeostatic ISGs than crypt-associated
452 cells, but that these homeostatic ISGs were expressed in a relatively small proportion of
453 enterocytes (< 20%) (**Figure 7B**). Notably, *Ifit1* (highlighted in red) was present in ~5% of
454 enterocytes by scRNA-seq, which is consistent with our observation of 1-4% *Ifit1*-positive area by
455 imaging the mouse small intestine (**Figures 6B-G**). Furthermore, the relative absence of ISG-
456 positive crypt-associated cells in this scRNA-seq data is consistent with our observation that
457 intestinal crypts lacked *Ifit1* and *Usp18* expression by imaging.

458 We expanded our investigation to a scRNA-seq dataset from the ileum of healthy, human,
459 pediatric patients that was previously described (Elmentaite et al., 2020). IECs from this dataset

460 were previously clustered by Elmentaite et al and annotated as: enterocytes, early enterocytes,
461 tuft cells, enteroendrocrine cells, BEST4 enterocytes, goblet cells, TA cells, and crypt. For our
462 analysis of homeostatic ISG expression, we excluded IEC sub-types with fewer than 20
463 constituent cells, which retained five annotated groups: enterocytes, early enterocytes, goblet
464 cells, TA cells, and crypt. Of the 21 homeostatic ISGs identified in **Figure 1D**, 14 orthologous
465 human genes were present in these data. Similar to analysis in **Figure 7A,** we determined the
466 percentage of each group that expressed each individual homeostatic ISG and generated a
467 heatmap of these data with hierarchical clustering to group IEC subtypes that have similar ISG
468 expression patterns (**Figure 7C**). Enterocyte, early enterocyte, and goblet subtypes clustered
469 separately from TA cells and crypt, with the highest proportion of homeostatic ISGs being present
470 in the enterocyte subtype (**Figure 7C**). As with mouse IEC data, above, we grouped annotated
471 cells that localize in the crypt (TA cells and crypt) and compared overall proportions of homeostatic
472 ISG expression with the mature enterocyte subtype (**Figure 7D**). Similar to mice, homeostatic
473 ISGs were present in significantly more enterocytes than crypt-associated cells, and most
474 homeostatic ISGs in this human dataset were present in a relatively small proportion of cells (<
475 20%). These human data suggest that ISGs may be present in a small proportion of IECs from
476 healthy, human ileal tissue at homeostasis and may share the localization observed in our murine
477 analyses. Our analysis of a murine scRNA-seq dataset support our previous observations that
478 homeostatic ISGs are not ubiquitously expressed throughout the intestinal epithelium; rather, they
479 are expressed in a minority of IECs and skewed towards mature enterocytes along the crypt-villus
480 axis. Our analysis of a human scRNA-seq dataset are consistent with observations in the murine
481 model, though future studies will be required to definitively address the existence of homeostatic
482 ISGs in human tissue.

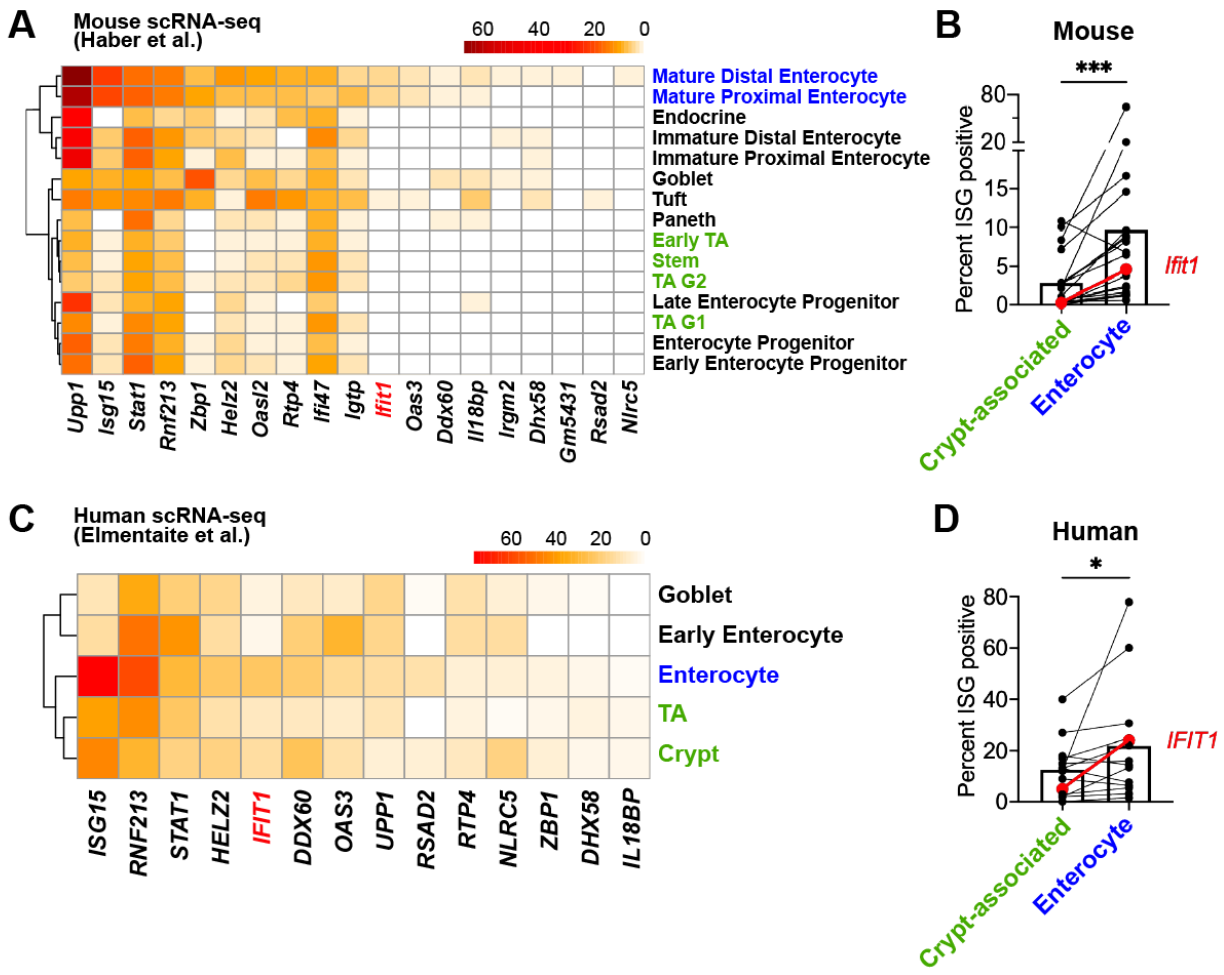

483

484 **Figure 7. Mature enterocytes express homeostatic ISGs in public single-cell datasets from**
485 **mouse and human. A-B.** A mouse IEC single-cell transcriptional dataset (Haber et al., 2017)
486 (GSE92332) was analyzed to determine the percentage of each epithelial cell subtypes that
487 express homeostatic ISGs. **A.** Heatmap depicting the proportion of each epithelial cell type
488 expressing nineteen of the twenty-one homeostatic ISGs identified in **Figure 1**. **B.** Enterocyte
489 subtypes (blue text) and crypt-resident progenitor subtypes (green text) cells were grouped and
490 the percentage of cells that express each homeostatic ISG was compared. **C-D.** A human IEC
491 single-cell transcriptional dataset (Elmentaite et al., 2020) (E-MTAB-8901) was analyzed for the
492 percentage of epithelial cell subtypes that express homeostatic ISGs. **C.** A heatmap depicting the
493 percentage of IEC subtypes that express human orthologs of murine homeostatic ISGs identified

494 in **Figure 1**. **D.** The mature enterocyte subtype (blue text) and crypt-resident progenitor subtypes
495 (green text) were grouped and the percentage of cells that express each homeostatic ISG was
496 compared. Lines in **B** and **D** link paired ISGs in each IEC subset. Statistical significance in **B** and
497 **D** was calculated by Wilcoxon test where * = $p < 0.05$, and *** = $p < 0.001$.
498

499 **Homeostatic ISG expression is partially restored by peroral LPS or flagellin in ABX-treated**
500 **mice**

501 To further define the relationship between bacteria and homeostatic ISGs, we assessed
502 whether oral administration of fecal contents or purified LPS (a bacterial MAMP and TLR4 agonist)
503 could restore localized ISG expression in mice with depleted bacterial microbiota. Control groups
504 of *Ifnlr1*$^{flox/flox}$ mice with conventional microbiota (**Figure 8A**) retained a localized *Ifit1* expression
505 pattern, whereas ABX-treated *Ifnlr1*$^{flox/flox}$ mice (**Figure 8B**) and *Ifnlr1*$^{\Delta IEC}$ mice (**Figure 8C**) lacked
506 *Ifit1* expression. Oral LPS administered to conventional *Ifnlr1*$^{flox/flox}$ mice did not significantly alter
507 the distribution or frequency of localized *Ifit1* expression (**Figure 8D**). However, localized *Ifit1*
508 expression was restored in a subset of ABX-treated *Ifnlr1*$^{flox/flox}$ mice administered LPS (**Figure**
509 **8E**). Fecal transplant of conventional microbes to ABX-treated *Ifnlr1*$^{flox/flox}$ mice was similarly
510 capable of restoring localized expression of *Ifit1* in a subset of mice (**Figure 8F**). Importantly, we
511 did not observe restoration of localized *Ifit1* expression in *Ifnlr1*$^{\Delta IEC}$ mice following LPS
512 administration (**Figure 8G**), indicating that restoration depends on IEC expression of *Ifnlr1*.

513 We noted that restoration of localized *Ifit1* signal following LPS administration or fecal
514 transplant appeared largely binary (i.e. present or absent) in our imaging data (**Figures 8E and**
515 **8F**, representative *Ifit1*-positive and *Ifit1*-negative images). Using quantification of *Ifit1* area
516 (**Figure 8H**), we stratified mice into *Ifit1*-postive and *Ifit1*-negative groups (**Figure 8I-J**) based on
517 a cut-off set at the maximal *Ifit1* area value of *Ifnlr1*$^{\Delta IEC}$ mice (dashed line in **Figure 8H**). This
518 analysis indicated 8/8 conventional *Ifnlr1*$^{flox/flox}$ mice, 0/8 ABX-treated control mice, 4/12 LPS-
519 treated mice, and 4/8 fecal transplant mice were *Ifit1*-positive (**Figure 8I-J**). Statistical analysis by

520 Fisher's exact test indicated that LPS administration non-significantly increased ($p = 0.1022$) the
521 proportion of mice that were *Ifit1*-positive, whereas fecal reconstitution of ABX-treated mice
522 significantly increased the likelihood of these mice being *Ifit1*-positive (**Figure 8J**). Importantly,
523 mice that received fecal transplant had full restoration of 16S gene copies (**Figure 8K**) despite
524 having partial restoration of homeostatic ISGs (4/8). These findings indicate that reconstitution of
525 homeostatic ISG signal has incomplete penetrance, underscoring the partial restoration by LPS
526 administration to ABX-treated mice.

527 To corroborate these findings, we performed orthogonal analyses of *Ifit1*, *Stat1*, and
528 *Oas1a* expression in ileum tissue of WT mice treated with ABX followed by fecal transplant, LPS
529 administration, administration of the TLR5 agonist: flagellin, or administration of TLR9 agonist:
530 CpG DNA (**Figure S9**). These data exhibited high variance, but were consistent with imaging data
531 in **Figure 8**, indicating a partial restoration of homeostatic ISGs in 20-50% of ABX-treated mice
532 by LPS, flagellin, or fecal transplant, but not CpG DNA (**Figure S9**). Together, these data indicate
533 that both LPS and flagellin are sufficient to restore homeostatic ISG expression to a similar extent
534 as total microbiota. The ability of multiple TLR stimuli to partially restore homeostatic ISGs
535 suggests that exposure to a variety of bacterial MAMPs is the basis for localized, homeostatic
536 ISG expression.

537

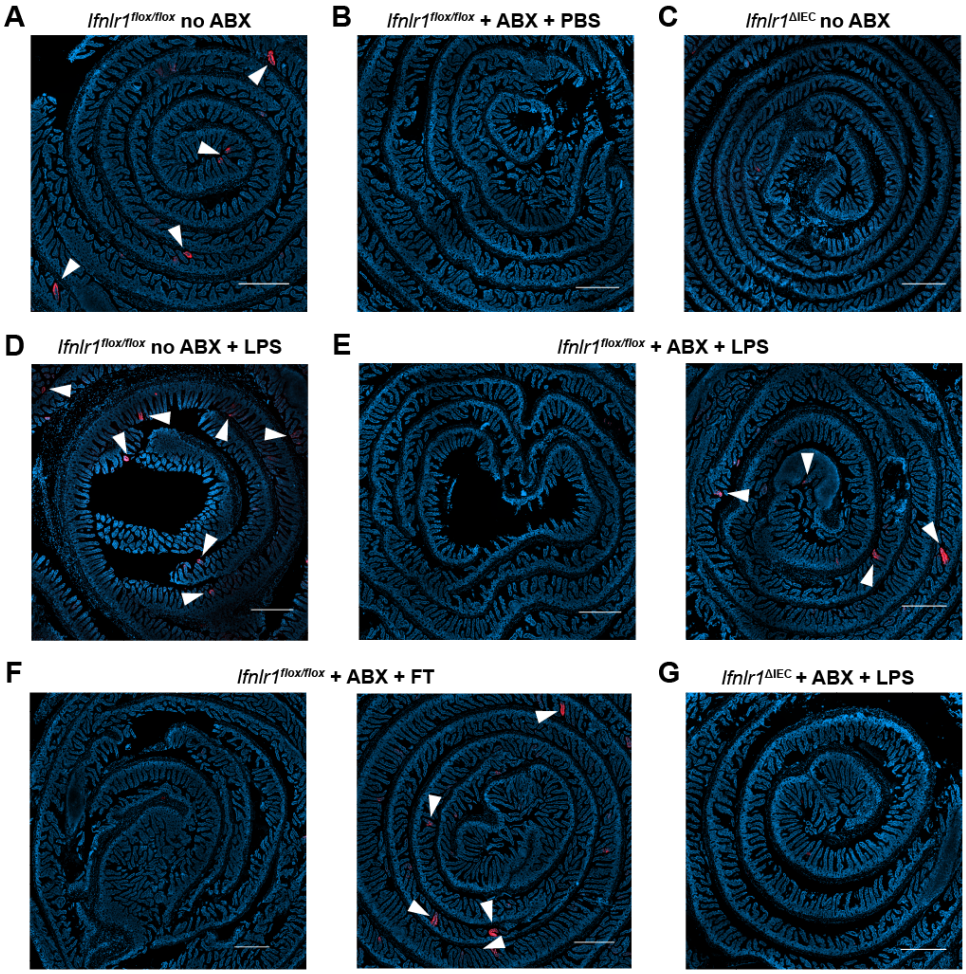

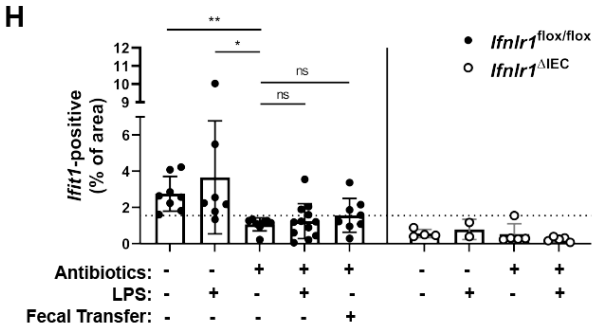

I

ABX	-	-	+	+	+
LPS	-	+	-	+	-
Fecal Transfer	-	-	-	-	+
Ifit1-positive mice / total	8/8	6/7	0/8	4/12	4/8

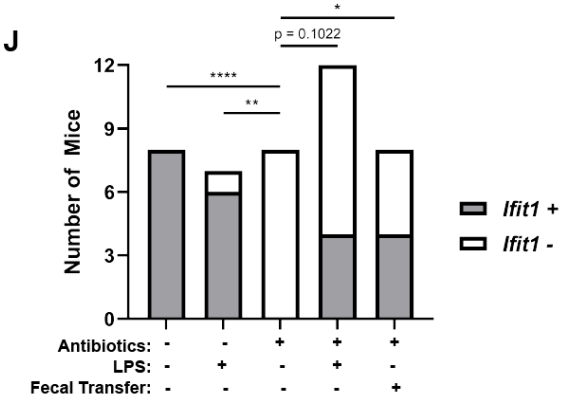

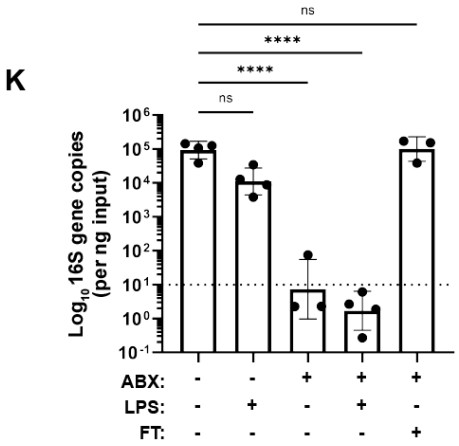

538 **Figure 8. Homeostatic ISG expression is partially restored by peroral LPS in ABX-treated**
539 **mice.** The ilea of treated WT, *Ifnlr1*$^{flox/flox}$, and *Ifnlr1*$^{\Delta IEC}$ mice were harvested, processed into Swiss
540 rolls, and stained by *in situ* hybridization for the ISG, *Ifit1* (red), with a DAPI (blue) counterstain**.**
541 **A-C.** Representative images from *Ifnlr1*$^{flox/flox}$ mice treated with H_2O control followed by PBS
542 stimulation **(A)**, ABX followed by PBS stimulation **(B)**, or from *Ifnlr1*$^{\Delta IEC}$ mice **(B)**. **D.**
543 Representative images of *Ifnlr1*$^{flox/flox}$ mice treated with H_2O control followed by LPS stimulation.
544 **E-F.** Two representative images of *Ifnlr1*$^{flox/flox}$ mice treated with ABX followed by LPS stimulation
545 **(E)** or ABX followed by fecal transplantation **(F)**. **G.** A representative image of *Ifnlr1*$^{\Delta IEC}$ mice
546 treated with ABX followed by LPS stimulation. **H.** Quantification of *Ifit1* area relative to the total
547 area of each tissue section with a dashed line at the highest *Ifnlr1*$^{\Delta IEC}$ value. The proportion of
548 *Ifit1*-positive mice (above dashed line) and *Ifit1*-negative mice (below dashed line) are tabulated
549 **(I)** and graphed **(J)** for *Ifnlr1*$^{flox/flox}$ mice of each condition. **K.** rDNA was isolated from the luminal
550 contents of mice at endpoint harvest. 16S gene copies were assessed by qPCR and normalized
551 to input. Limit of detection: dashed line. Where depicted, scale bar = 500μm. Data points represent
552 individual mice and are pooled from 4 independent experiments in **A-J** and from 2 independent
553 experiments in **K**. Statistical significance was determined by Kruskal-Wallis with Dunn's multiple
554 comparisons in **H**, by one-way ANOVA with Dunnett's multiple comparisons in **K**, and by Fisher's
555 exact tests in **J** where * = $p < 0.05$, ** = $p < 0.01$, and **** = $p < 0.0001$.

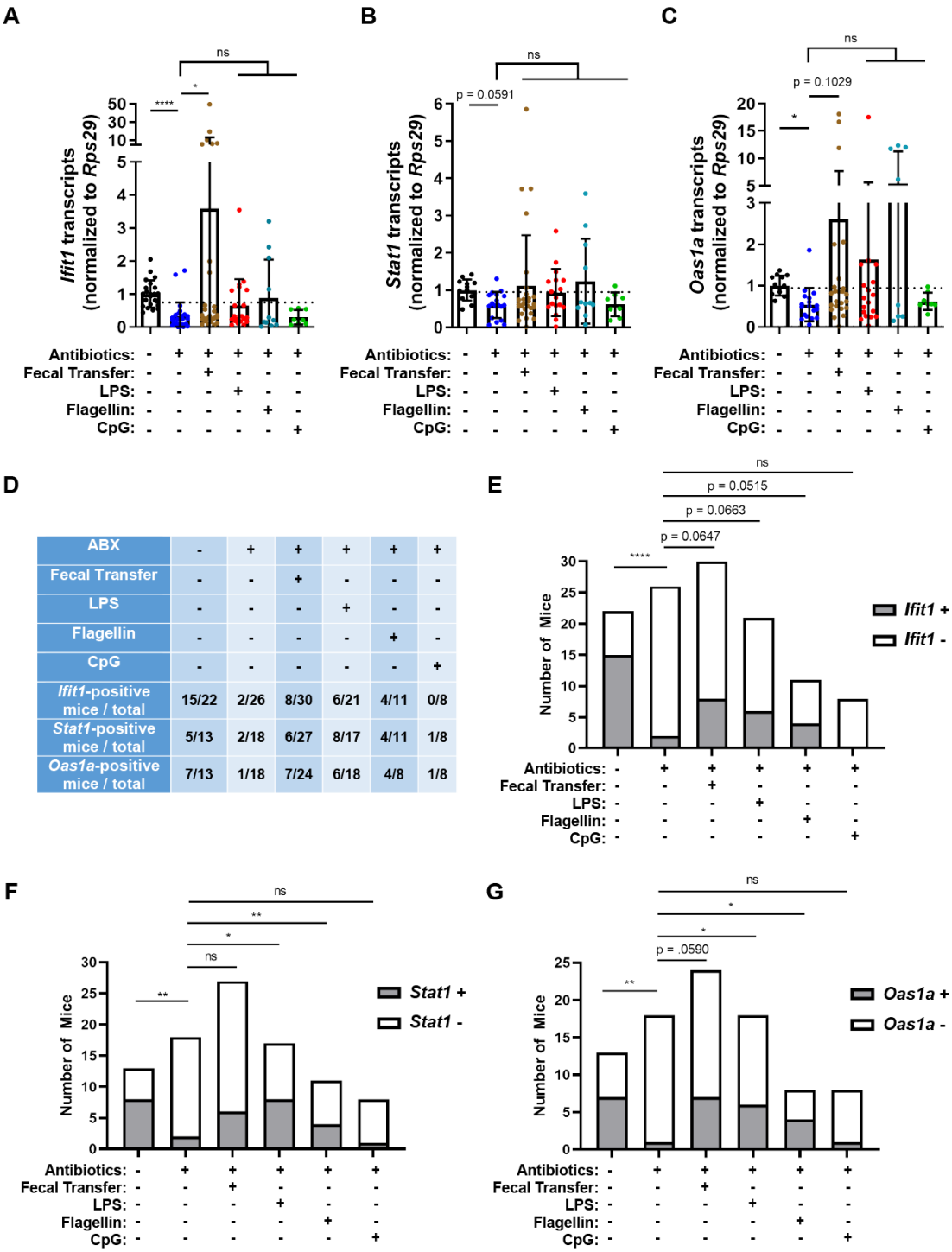

ABX	-	+	+	+	+	+
Fecal Transfer	-	-	+	-	-	-
LPS	-	-	-	+	-	-
Flagellin	-	-	-	-	+	-
CpG	-	-	-	-	-	+
Ifit1-positive mice / total	15/22	2/26	8/30	6/21	4/11	0/8
Stat1-positive mice / total	5/13	2/18	6/27	8/17	4/11	1/8
Oas1a-positive mice / total	7/13	1/18	7/24	6/18	4/8	1/8

556

557 **Figure S9. Homeostatic ISG expression is partially restored by peroral LPS in ABX-treated**

558 **mice.** The ileum of treated WT, *Ifnlr1*$^{flox/flox}$, and *Ifnlr1*$^{\Delta IEC}$ mice was harvested and *Ifit1* **(A)**, *Stat1*

559 **(B)**, and *Oas1a* **(C)** was quantified by qPCR. Delineation of positive ISG expression was

560 conservatively selected as one standard deviation above the mean of ABX-treated mice (dashed
561 line). Mice were binned into ISG-positive (above dashed line) or ISG-negative (below dashed line)
562 groups and are tabulated for each condition in **D**. The proportion of mice with expression of *Ifit1*
563 **(E)**, *Stat1* **(F)**, and *Oas1a* **(G)** are graphed for each condition. Data points represent individual
564 mice and are pooled from 3-9 independent experiments. Statistical significance was determine
565 by Kruskal-Wallis with Dunn's multiple comparisons **(A-C)** and by Fisher's exact test **(E-G)** where
566 * = $p < 0.05$, ** = $p < 0.01$, and **** = $p < 0.0001$.
567

568 **The homeostatic IFN-λ response preemptively protects IECs from murine rotavirus**
569 **infection**

570 To assess the capacity of homeostatic ISGs to protect IECs from viral infection, we utilized
571 infection with murine rotavirus (mRV), an IEC-tropic pathogen. Prior studies of rotaviruses have
572 identified viral immune evasion genes that block IFN induction through multiple mechanisms
573 (Arnold et al., 2013). However, we reasoned that pre-existing ISG expression stimulated by the
574 bacterial microbiome at homeostasis may preemptively protect IECs from the infection before
575 viral gene expression is initiated. To determine the role of an epithelial IFN-λ response over the
576 course of mRV infection in adult mice, we monitored daily shedding of viral genomes in the stool
577 of *Ifnlr1*$^{flox/flox}$ mice and *Ifnlr1*$^{\Delta IEC}$ littermates. We first detected mRV shedding in the stool on day
578 two after inoculation and, at this early timepoint, *Ifnlr1*$^{\Delta IEC}$ mice shed 20-fold more mRV genomes
579 into their stool than *Ifnlr1*$^{flox/flox}$ mice (**Figure 9A**). However, at the peak of viral shedding between
580 days three and five, there were no significant differences between *Ifnlr1*$^{flox/flox}$ and *Ifnlr1*$^{\Delta IEC}$
581 littermates (**Figure 9A**). This similarity at peak of viral shedding was consistent with an ability of
582 mRV to evade the host IFN response once infection is established. Together, these findings
583 suggest that *Ifnlr1*$^{\Delta IEC}$ mice have defects in protection against initiation of mRV infection and that
584 the protective capacity of endogenous IFN-λ signaling against mRV is primarily prophylactic in
585 nature.

586 To more stringently assess the capacity of *Ifnlr1* to protect IECs against the earliest stages
587 of mRV infection, we inoculated mice with 5000 SD50 (50% shedding dose) of mRV to maximize
588 the likelihood of uniform viral exposure throughout the intestine. At 12 and 24 hours post-
589 inoculation, we quantified mRV genomes in the ileum and the proportion of infected IECs (live,
590 EpCAM-positive, CD45-negative, and mRV-positive) by flow cytometry. At 24 hours post-
591 inoculation, we found that *Ifnlr1*$^{\Delta IEC}$ mice had 20-fold more mRV genomes than *Ifnlr1*$^{flox/flox}$ mice
592 (**Figure 9B**). In addition, we found that a three-fold greater proportion of IECs were infected with
593 mRV in *Ifnlr1*$^{\Delta IEC}$ mice than *Ifnlr1*$^{flox/flox}$ mice at 24 hours post-infection (**Figures 9C-F**). However,
594 the median fluorescence intensity (MFI) of mRV antigen was equivalent in mRV-infected IECs
595 from *Ifnlr1*$^{flox/flox}$ and *Ifnlr1*$^{\Delta IEC}$ mice (**Figure 9G**) and the MFI of mRV did not correlate ($r^2 = 0.0003$)
596 with the percentage of infected IECs (**Figure 9H**). This equivalent mRV antigen burden in infected
597 cells from *Ifnlr1*$^{flox/flox}$ and *Ifnlr1*$^{\Delta IEC}$ mice in combination with the lack of correlation between antigen
598 burden and percentage of infected cells suggests that the protective role of *Ifnlr1* is to prevent
599 infection of IECs rather than to limit replication within IECs after they are infected. To further
600 contextualize the role of homeostatic ISGs in protection against mRV, we performed *in situ*
601 hybridization for both mRV and *Ifit1* in the ileum of WT mice at 24 hours post-inoculation (**Figure**
602 **9I**). We observed variability in the magnitude of mRV infection between mice at this timepoint;
603 however, we generally found that mRV RNA was not present in villi that have *Ifit1* expression.
604 Additionally, we found mRV infection did not dramatically increase area of *Ifit1* expression in the
605 intestine at 24 hours post-inoculation. However, at 96 hours post-inoculation, we found a
606 significant increase in epithelial *Ifit1* expression in the ileum relative to early times post-inoculation
607 (**Figure S10**). These data are consistent with previously described mRV evasion of IFN responses
608 within infected cells (Arnold et al., 2013), and suggest that *Ifit1* expression at 24 hours post-
609 inoculation is due to the preexisting homeostatic response.

610 We assessed an earlier timepoint at 12 hours post-inoculation and observed similar trends
611 toward an increased proportion of IEC infection in *Ifnlr1*$^{\Delta IEC}$ relative to *Ifnlr1*$^{flox/flox}$ littermates, but

612 the extent of infection was 10-100 fold lower and near the limit of detection (**Figure S11**). Thus
613 12- and 24-hour timepoints capture the earliest detectable infection of IECs by mRV. Together
614 these data indicate that *Ifnlr1* expression by IECs reduces the proportion of cells initially infected
615 by mRV, but does not limit the extent of replication once infection is established, consistent with
616 an early protective role for homeostatic ISG expression that preempts viral IFN evasion
617 mechanisms.

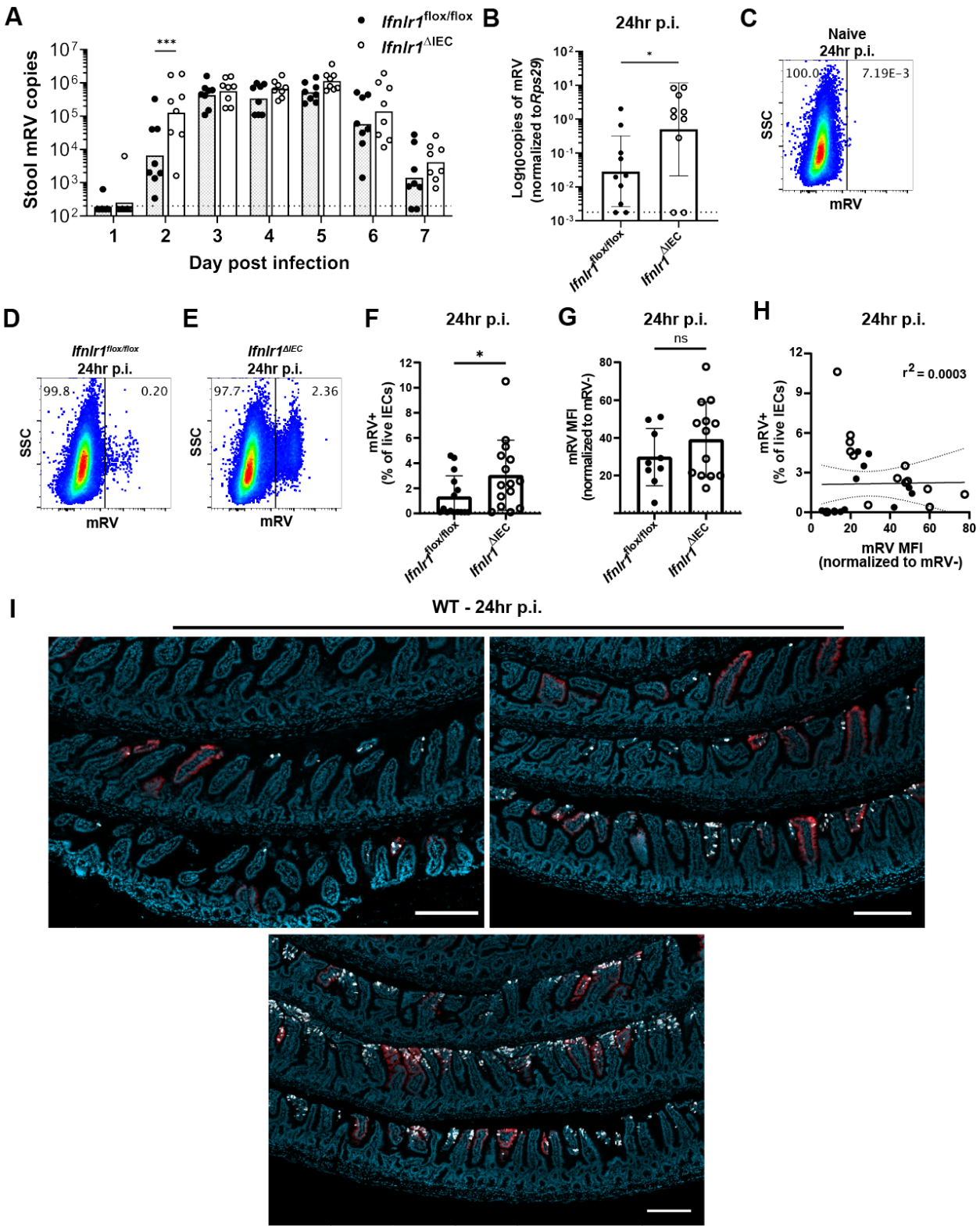

618

619 **Figure 9. The homeostatic IFN-λ response preemptively protects IECs from murine**

620 **rotavirus infection.** *Ifnlr1*$^{flox/flox}$ and *Ifnlr1*$^{\Delta IEC}$ mice were infected with 100 SD50 **(A)** or 5000 SD50

621 **(B-H)** of mRV and stool **(A)** or stripped ileal intestinal epithelial cells **(B-G)** were assessed for
622 mRV infection. **A.** Timecourse of mRV genome copies detected in the stool of *Ifnlr1*$^{flox/flox}$ and
623 *Ifnlr1*$^{\Delta IEC}$ mice by qPCR. **B-G.** Mechanically stripped intestinal epithelial cell fractions were
624 analyzed by qPCR for mRV genome copies **(B)** or flow cytometry for RV antigen-positive IECs
625 **(C-G).** Representative flow cytometry plots of naïve **(C)**, *Ifnlr1*$^{flox/flox}$ **(D)**, and *Ifnlr1*$^{\Delta IEC}$ **(E)** mice
626 infected with mRV with quantification in **(F)**. **G.** The MFI of mRV antigen in infected cells relative
627 to uninfected cells. **H.** A linear correlation plot of mRV+ cells and mRV MFI with 95% confidence
628 intervals (dashed lines). **I.** WT mice were infected with 5000 SD50 of mRV and the ilea were
629 processed into Swiss rolls and stained by *in situ* hybridization for the ISG, *Ifit1* (red), or murine
630 rotavirus (white), with a DAPI (blue) counterstain. Representative images depicting varying
631 degrees of infection. Scale bar = 200μm. Where designated in **A-G**, dashed lines = LOD as set
632 by naïve mice. Data points represent individual mice and are pooled from 2 independent
633 experiments in **A-B** and 3 independent experiments in **C-H**. Images in **I** are representative of 10
634 mice from 2 independent experiments. Statistical significance was determined by two-way
635 ANOVA with Sidak's multiple comparisons **(A)**, by Mann Whitney **(B, F)**, or unpaired t-test **(G)**
636 where * = $p < 0.05$, *** = $p < 0.001$.

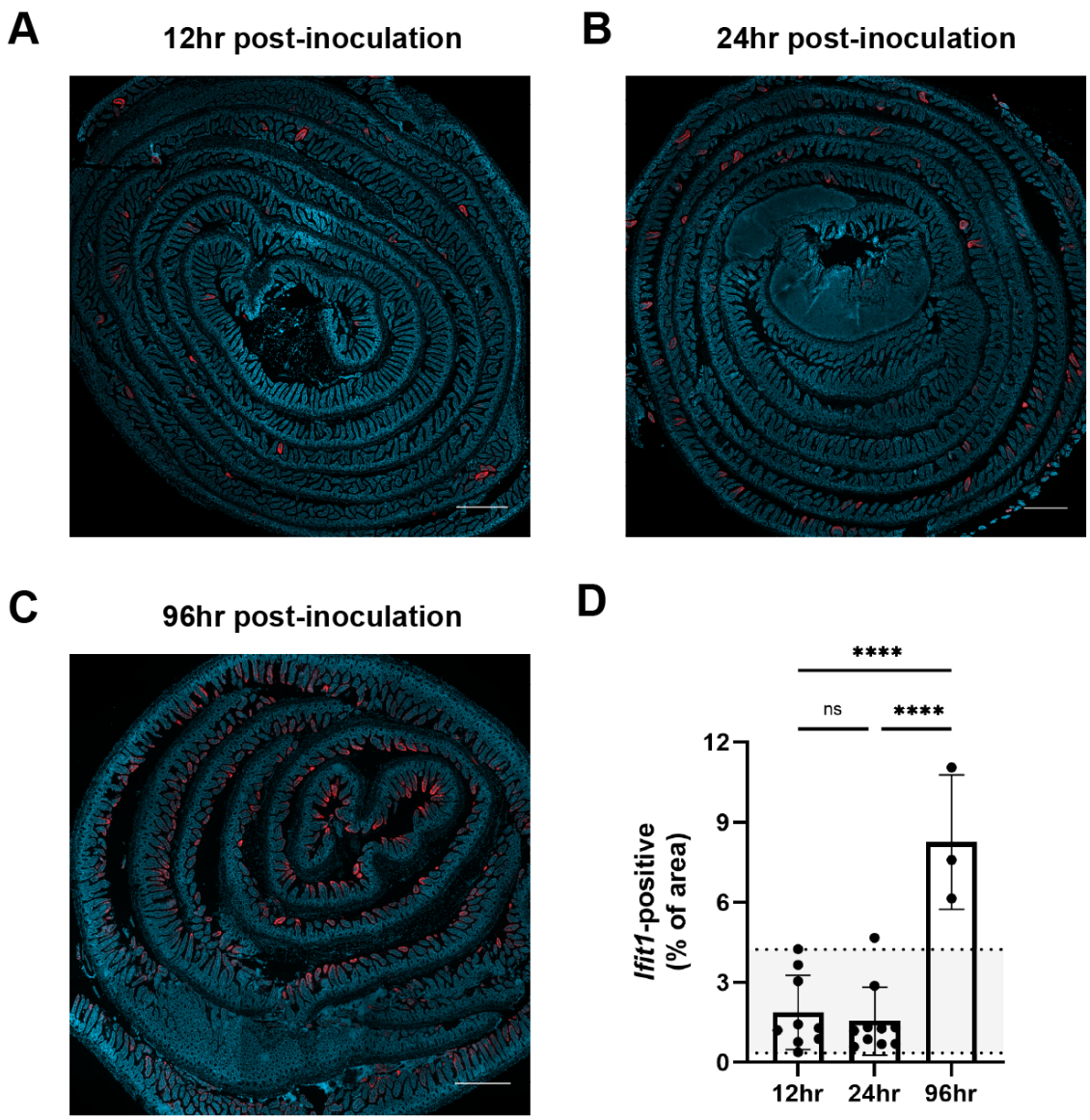

637

638 **Figure S10. Murine rotavirus infection increases the distribution of *Ifit1* expression at late**
639 **times post-inoculation.** WT mice were infected with 5000 SD50 of mRV and the ilea were
640 processed into Swiss rolls and stained by *in situ* hybridization for the ISG, *Ifit1* (red) with a DAPI
641 (blue) counterstain. Representative images at **(A)** 12hr post-inoculation, **(B)** 24hr post-inoculation,
642 and **(C)** 96hr post-inoculation. Quantification of *Ifit1* area relative to the total area of each tissue
643 section with highlighted area representing historical range of *Ifit1* area in uninfected WT mice.
644 Where displayed, scale bar = 500μm. Data points represent individual mice and are pooled from
645 two independent experiments for 12hr and 24hr timepoints, and one experiment for the 96hr

timepoint. Statistical significance was determined by one-way ANOVA with Tukey's multiple comparisons where **** = p < 0.0001.

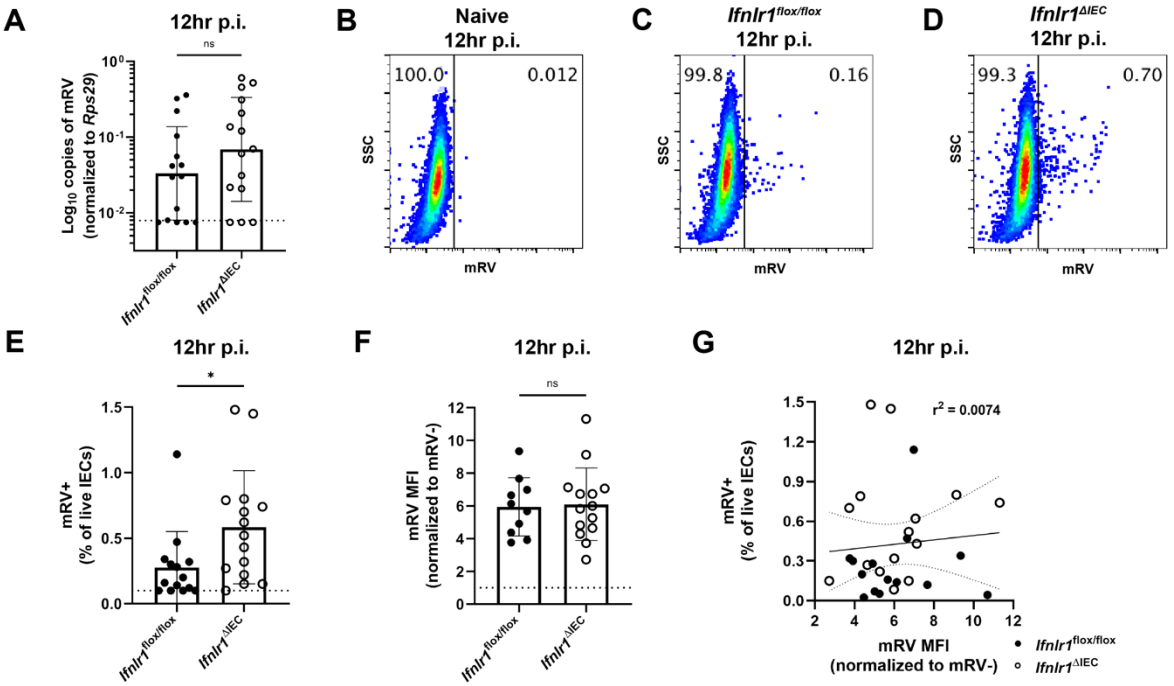

Figure S11. The homeostatic IFN-λ response preemptively protects IECs from murine rotavirus infection. *Ifnlr1*$^{flox/flox}$ and *Ifnlr1*$^{\Delta IEC}$ mice were infected with 5000 SD50 of mRV by oral gavage and stripped ileal intestinal epithelial cell fractions were analyzed by qPCR for mRV genome copies **(A)** or flow cytometry for RV antigen-positive IECs **(B-F)**. Representative flow cytometry plots of naïve **(B)**, *Ifnlr1*$^{flox/flox}$ **(C)**, and *Ifnlr1*$^{\Delta IEC}$ **(D)** mice infected with mRV. **F.** The MFI of mRV antigen in infected cells relative to uninfected cells. **G.** A linear correlation plot of mRV+ cells and mRV MFI with 95% confidence intervals (dashed lines). Data points represent individual mice and are pooled from 3 independent experiments. Statistical significance was calculated by Mann Whitney **(A, E)**, or unpaired t-test **(F)** where * = p < 0.05.

658 **Discussion**

659 Here, we report that bacterial microbiota induce an enteric IFN-λ response in IECs at
660 homeostasis (**Figures 1-4**). Although there are previous reports of basal, non-receptor-dependent
661 ISG expression in immortalized and primary cell lines (Hakim et al., 2018), the homeostatic
662 response that we report here is dependent on the IFN-λ receptor. Furthermore, we find this
663 response is independent of type I IFN signaling (**Figure 3**), indicating that IFN-λ signaling plays a
664 dominant and active role in the gastrointestinal epithelium. We also find minimal changes in ISG
665 expression within the spleen and MLN after ABX treatment, suggesting that homeostatic ISGs
666 are predominantly expressed in the intestine. These findings differ slightly from prior descriptions
667 of systemic type I IFN responses that are dependent on bacterial microbiota (Abt et al., 2012;
668 Bradley et al., 2019; Ganal et al., 2012; Steed et al., 2017; Stefan et al., 2020; Winkler et al.,
669 2020). However, differences in the specific tissues and cell types analyzed make it difficult to draw
670 direct comparisons across these studies. Therefore, we conclude that homeostatic ISGs are
671 substantially present in IECs, but do not dispute the prior findings that relatively low homeostatic
672 ISG expression induced by type I IFN plays an important role in extra-intestinal tissues and non-
673 epithelial cell types.

674 A prior study by Mahlakõiv et al. noted the presence of *Ifnl2/3* transcripts in CD45+ cells
675 within the stripped intestinal epithelium, but not the lamina propria, at homeostasis. We have
676 confirmed these findings and have extended them to show that this homeostatic expression of
677 *Ifnl2/3*, but not *Ifnb1*, is dependent on bacterial microbiota (**Figure 5**). However, we have been
678 unable to detect IFN-λ transcripts by RNA scope *in situ* hybridization in mice at homeostasis,
679 consistent with recently published data (Ingle et al., 2021). This suggests that the production of
680 IFN-λ is below the limit of detection by imaging or highly transient in nature. It is also unclear
681 which CD45+ cell type produces homeostatic IFN-λ. Swamy et al. showed that T cell receptor
682 stimulation led intraepithelial lymphocytes to produce IFN-λ (Swamy et al., 2015) and Mahlakõiv
683 et al. suggested that the primary producers of IFN-λ at steady-state are intraepithelial lymphocytes

684 due to the abundance of intraepithelial lymphocytes in the epithelial fraction. However, myeloid
685 cells also reside near the intestinal epithelium and can sample luminal contents by various
686 mechanisms (Chieppa et al., 2006; McDole et al., 2012; Niess et al., 2005). Although the cell type
687 that produces homeostatic IFN-λ is unknown, enrichment for *Ifnl2/3* in CD45+ cells within the
688 intestinal epithelial fraction suggests that proximity to bacterial stimuli may be a primary
689 determinant in this response. We suggest that these cells may be actively surveying the intestinal
690 epithelium to detect bacterial MAMPs. The specific CD45+ cell types responsible for producing
691 homeostatic IFN-λ will be a topic of interest for future studies.

692 We initially anticipated that the distribution of homeostatic ISGs would be uniform among
693 IECs. Instead, we found that this IFN-λ response is highly localized within enteric tissues.
694 Homeostatic ISGs are observed in a minority of small intestinal villi and are primarily present in
695 mature epithelium towards the villus tips (**Figure 6**). Likewise, homeostatic ISGs are present
696 within patches of the mature epithelium in the colon (**Figure S8**). The surprising finding of
697 localized ISGs in the ileum are supported by analysis of independently-generated scRNA-seq
698 datasets from mouse and human small intestinal IECs that depict expression of homeostatic ISGs
699 in a minority of cells with predominant expression in mature enterocytes (**Figure 7**). The basis for
700 this pattern is unknown; however, it may reflect the distribution of cells capable of sensing
701 bacterial microbiota, distinct microenvironments within the gastrointestinal tract, or qualitative
702 differences in bacterial colonization. Further delineation of the factors that render specific regions
703 "responsive" will be of great interest for follow-up studies.

704 Our finding that LPS administration, flagellin administration, or fecal transplant can
705 partially restore the expression of homeostatic ISGs in the small intestine (**Figures 8** and **Figure**
706 **S9**) supports the concept that localized ISG-positive regions are uniquely exposed or responsive
707 to a variety of bacterial MAMPs. Indeed, we find that MYD88 is required for WT levels of
708 homeostatic ISG expression in the small intestine (**Figure 3**). However, MYD88 is dispensable
709 for homeostatic ISG expression in the colon, and TRIF is not required in either small intestine or

710 colon (**Figure 3**). These data suggest that the bacterial microbiota broadly stimulates homeostatic
711 IFN-λ through multiple, redundant PRRs. Furthermore, localized restoration of ISGs following LPS
712 administration (**Figure 8**) suggests that localization is an intrinsic property of homeostatic ISG
713 stimulation and is not likely to be due to qualitative differences in bacterial colonization. ISG
714 localization may be indicative of regional differences in access of luminal bacterial MAMPs to IFN-
715 λ-producing cells. One host mechanism to limit bacterial interactions with the intestinal epithelium
716 is the presence of mucus layers (Atuma et al., 2001; Johansson et al., 2011). Intriguingly, the
717 single mucus layer in the small intestine is much less adherent than the mucus layers present in
718 the colon (Johansson et al., 2011), which might allow occasional direct bacterial interactions with
719 IECs or other cells near the intestinal epithelium. However, soluble components from enteric
720 bacteria may also readily diffuse through mucus layers. In this case, there may be sporadic
721 defects in tight junction proteins that are required to maintain the intestinal epithelium. Tight
722 junction remodeling is essential to maintain intestinal integrity during apoptosis and extrusion of
723 IECs that are regularly shed from the intestinal epithelium (Williams et al., 2015). Future studies
724 will be necessary to determine whether defects in epithelial barrier integrity during extrusion
725 events are linked to the local ISG responses that we observe.

726 The preceding findings (**Figure 4)** suggested that the homeostatic ISG response in IECs
727 would provide protection against IEC-tropic viruses, such as mRV. Although bacterial-associated,
728 IFN-independent mechanisms of mRV clearance have been reported (Shi et al., 2019; Zhang et
729 al., 2014), we found that the signature of homeostatic ISGs in ileum tissue included well-
730 characterized antiviral ISGs (**Figures 1-2**). To investigate whether these homeostatic ISGs
731 protect against MRV, we used *Ifnlr1*$^{\Delta IEC}$ mice that lack homeostatic ISGs (**Figure 4 and 6**) rather
732 than using ABX-treatment, which introduces pleiotropic effects on rotavirus infection (Uchiyama
733 et al., 2014) and dramatically increases transit time through the intestine (Baldridge et al., 2015).
734 Using *Ifnlr1*$^{\Delta IEC}$ mice, we found increase in IEC infection by mRV at early stages of infection
735 compared to *Ifnlr1*$^{flox/flox}$ littermates (**Figure 9**). However, the protection offered by IEC expression

736 of *Ifnlr1* was lost by the middle and late stages of infection, consistent with the ability of mRV to
737 antagonize induction of IFN responses once infection is established (Arnold et al., 2013). Our
738 observations during initiation of infection may provide important context to observations in other
739 studies that report differing capacity for infection-induced IFN-λ to protect against mRV infection
740 (Lin et al., 2016; Pott et al., 2011). Ultimately, it is clear that prophylactic administration of
741 exogenous IFN-λ protects against mRV infection (Lin et al., 2016; Pott et al., 2011; Van Winkle et
742 al., 2020), indicating that homeostatic IFN-λ is also protective when induced by bacterial
743 microbiota prior to infection. In sum, these findings indicate that preexisting, homeostatic ISGs
744 present in *Ifnlr1*-sufficient mice are protective during initiation of mRV infection, but that
745 endogenous IFN-λ does not reduce mRV burden in infected cells. These data highlight the
746 possibility that detection of bacterial microbiota in particularly exposed areas may preemptively
747 activate homeostatic ISGs as a form of anticipatory immunity to protect the intestinal epithelium
748 from enteric viruses.

749 **Methods**

750 **Mice**

751 All mice were bred using the C57BL/6 background and used within the age of 8-12 weeks;
752 C57BL/6J mice (stock # 000664) were purchased from Jackson Laboratories (Bar Harbor, ME)
753 and used as wild-type. Genetically modified mice included *Ifnlr1*$^{-/-}$ and *Ifnlr1*$^{flox/flox}$ (generated from
754 *Ifnlr1*$^{tm1a(EUCOMM)Wtsi}$ as published (Baldridge et al., 2017)), *Ifnar1*$^{-/-}$ (B6.129.Ifnar1^{tm1}), *Trif*$^{-/-}$ (JAX
755 C57BL/6J-*Ticam1*^{Lps2}/J, stock #005037), *Myd88*$^{-/-}$ (JAX B6.129P2(SJL)-*Myd88*$^{tm1.1Defr}$/J, stock
756 #009088), *Irf3*$^{-/-}$ (B6.129S/SvEv-Bcl2l12/Irf3^{tm1Ttg}), *Irf7*$^{-/}$ (B6.129P2-Irf7tm1Ttg/TtgRbrc), *Stat1*$^{-/-}$
757 (B6.129.-*Stat1*^{tm1Dlv}), and Villin-cre (B6.Cg-Tg(Vil1-cre)997Gum/J) mice. *Ifnlr1*$^{-/-}$ and *Ifnar1*$^{-/-}$ mice
758 were bred to *Ifnlr1*^{Het}/*Ifnar1*^{Het} mice to generate littermate *Ifnlr1*^{Het}/*Ifnar1*^{Het}, *Ifnlr1*^{Het}/*Ifnar1*^{KO},
759 *Ifnlr1*^{KO}/*Ifnar1*^{Het}, *Ifnlr1*^{KO}/*Ifnar1*^{KO} offspring.

760 All mice were maintained in specific-pathogen-free facilities at Oregon Health & Science
761 University (OHSU) and Washington University in St. Louis (WUSTL). Animal protocols were
762 approved by the Institutional Animal Care and Use Committee at OHSU (protocol #IP00000228)
763 and WUSTL (protocol #20190162) in accordance with standards provided in the *Animal Welfare*
764 *Act*.

765 For all experiments, mice were allocated into experimental groups based on genotype with
766 equal representation of individual litters and equal sex ratios.

767 **Mouse Treatments**

768 Mice were administered an *ad libitum* antibiotic cocktail consisting of: 1 g/L ampicillin, 1
769 g/L metronidazole, 1 g/L neomycin, and 0.5 g/L vancomycin (Sigma, St. Louis, MO) in autoclaved
770 H_2O (OHSU) or in 20 mg/mL grape Kool-Aid (Kraft Foods, Northfield, IL) (WUSTL). Sterile H_2O
771 (OHSU) or Kool-Aid (WUSTL) alone was used as a control. Mice were maintained on antibiotics
772 or control for 2 weeks prior to harvest.

773 Recombinant IFN-λ was provided by Bristol-Myers Squibb (New York City, NY) as a
774 monomeric conjugate comprised of 20kDa linear PEG attached to the amino-terminus of murine

775 IFN-λ. Mice were injected intraperitoneally with IFN-λ or an equal volume of PBS vehicle as
776 indicated in figure legends at the indicated time prior to analysis.

777 Mice were stimulated with of 100μg of the synthetic dsRNA analogue, poly I:C (R&D,
778 #4287) or PBS by intraperitoneal injection in a 200μL volume, 2 hours prior to harvest.

779 25μg of the bacterial product lipopolysaccharide (Sigma #L4391), flagellin (Invivogen #tlrl-
780 bsfla; from *Bacillus subtilis*) or CpG (Invivogen #tlrl-1585; Class A CpG oligonucleotide) were
781 perorally administered to mice in 25μL of sterile PBS. Mice were treated on days 15 and 16 of
782 antibiotic treatment or H_2O control prior to harvest on day 17.

783 For transplantation of fecal material, antibiotic treatment was stopped and mice were fed
784 25uL of fecal mixture by pipet for two consecutive days. Fecal mixture was prepared by collecting
785 fecal samples from control mice; a single stool pellet was resuspended in 200uL of sterile PBS,
786 stool was broken apart by pipetting, and large particulate was allowed to settle for several minutes
787 prior to administration.

788 **Cell Isolation**

789 Epithelial fractions were prepared by non-enzymatic dissociation as previously described
790 (Nice et al., 2016). Briefly, mouse ileum was opened longitudinally and agitated by shaking in
791 stripping buffer (10% bovine calf serum, 15 mM HEPES, 5 mM EDTA, and 5 mM dithiothreitol
792 [DTT] in PBS) for 20 min at 37°C. Lamina propria fractions were prepared by enzymatic digestion
793 and dissociation with the Lamina Propria Dissociation Kit and GentleMacs Dissociator (Miltenyi
794 Biotec, Bergisch Gladbach, Germany). Dissociated cells were collected for use in qPCR analysis,
795 flow cytometry, and magnet enrichment.

796 **Rotavirus infection of mice**

797 Mouse rotavirus (EC strain) was graciously provided by Andrew Gewirtz (Georgia State
798 University). Viral stocks were generated by inoculating 4- to 6-day-old neonatal BALB/c mice and
799 harvesting the entire gastrointestinal tract upon presentation of diarrheal symptoms 4 to 7 days
800 later. Intestines were freeze-and-thawed, suspended in PBS, and homogenized in a bead beater

801 using 1.0-mm zirconia-silica beads (BioSpec Products). These homogenates were clarified of
802 debris, aliquoted, and stored at -70°C. The 50% shedding dose (SD50) was determined by
803 inoculation of 10-fold serial dilutions in adult C57BL/6J mice. For stool time-course studies, mice
804 were inoculated by peroral route with 100 SD50 and a single stool pellet was collected daily for
805 viral quantitation by qPCR. For protection studies, mice were inoculated by intragastric gavage
806 with 5000 SD50, and ileum was isolated and mechanically stripped 12- and 24-hours later for
807 quantitation of viral burden by qPCR and flow cytometry.

808 **RNA isolation, rDNA isolation, qPCR, and analysis**

809 RNA from tissue and stripped IECs was isolated with TRIzol (Life Technologies, Carlsbad,
810 CA) according to the manufacturer's protocol. RNA from magnet-enriched cells was purified by
811 Zymo *Quick*-RNA Viral Kit (Zymo Research, Irvine, CA). The larger of either 1µg of RNA or 5µL
812 of RNA were used as a template for cDNA synthesis by the ImProm-II reverse transcriptase
813 system (Promega, Madison, WI) after DNA contamination was removed with the DNAfree kit (Life
814 Technologies). 16S bacterial rDNA was isolated from stool and intestinal contents with a
815 ZymoBIOMICS DNA kit (Zymo Research, Irvine, CA) kit. Quantitative PCR was performed using
816 PerfeCTa qPCR FastMix II (QuantaBio, Beverly, MA) and the absolute quantities of transcript
817 were determined using standard curves composed of gBlocks (IDT) containing target sequences.
818 Absolute copy numbers from tissue samples were normalized to the housekeeping gene,
819 ribosomal protein S29 (*Rps29*). Taqman assays for selected genes were ordered from IDT
820 (Coralville, IA): *Rps29* (Mm.PT.58.21577577), *Ifit1* (Mm.PT.58.32674307), *Oas1a*
821 (Mm.PT.58.30459792), *Mx2* (Mm.PT.58.11386814), *Stat1* (Mm.PT.58.23792152), *Isg15*
822 (Mm.PT.58.41476392.g). Taqman assays for *Ifnl2/3* and *Ifnb1* were designed previously (Van
823 Winkle et al., 2020) and consisted of the following primer-probe sequences: *Ifnl2/3* (Primer 1 –
824 GTTCTCCCAGACCTTCAGG, Primer 2 – CCTGGGACCTGAAGCAG, Probe –
825 CCTTGCAGGCTGAGGTGGC); *Ifnb1* (Primer 1 – CTCCAGCTCCAAGAAAGGAC, Primer 2 –
826 GCCCTGTAGGTGAGGTTGAT, Probe – CAGGAGCTCCTGGAGCAGCTGA). Murine rotavirus

827 was detected using Taqman primer-probe sets specific for 422-521 of GeneBank sequence
828 DQ391187 as previously described (Fenaux et al., 2006) with the following sequences: Primer 1
829 – GTTCGTTGTGCCTCATTCG, Primer 2 – TCGGAACGTACTTCTGGAC, Probe –
830 AGGAATGCTTCAGCGCTG; and universal bacterial 16S rDNA was detected using Taqman
831 primer-probe sets with previously designed sequences (Nadkarni et al., 2002): Primer 1 –
832 GGACTACCAGGGTATCTAATCCTGTT, Primer 2 – TCCTACGGGAGGCAGCAGT, Probe –
833 CGTATTACCGCGGCTGCTGGCAC.

834 **RNAscope**

835 Swiss rolls of intestinal tissue were fixed in 10% neutral-buffered formalin for 18-24hr and
836 paraffin-embedded. Tissue sections (5μm) were cut and maintained at room temperature with
837 desiccant until staining. RNA *in situ* hybridization was performed using the RNAscope Multiplex
838 Fluorescent v2 kit (Advanced Cell Diagnostics, Newark, CA) per protocol guidelines. Staining with
839 anti-sense probes for detection of *Ifit1* (ACD, #500071-C2), *Usp18* (ACD, #524651-C1) and MRV
840 (ACD, #1030611-C1) was performed using ACDBio protocols and reagents. MRV probes were
841 designed to target 2-1683 of DQ391187 against NSP3, VP7, and NP4. Slides were stained with
842 DAPI and mounted with ProLong Gold antifade reagent (ThermoFisher), and imaged using a
843 Zeiss ApoTome2 on an Axio Imager, with a Zeiss AxioCam 506 (Zeiss).

844 **Flow Cytometry and Magnet Enrichment**

845 Dissociated cells were collected and stained for flow cytometry. Cells were stained with
846 Zombie Aqua viability dye (BioLegend), Fc receptor-blocking antibody (CD16/CD32; BioLegend),
847 anti-EpCAM (clone G8.8; BioLegend), and anti-CD45 (clone 30-F11; BioLegend). For analysis of
848 murine rotavirus infection, cells were stained with anti-rotavirus (polyclonal; ThermoFisher, #PA1-
849 7241) followed by goat anti-rabbit secondary (ThermoFisher). All data were analyzed using
850 FlowJo software (BD Biosciences). Gates were set based on unstained and single-fluorophore
851 stains. IECs were selected by gating on live, EpCAM-positive, CD45-negative cells. Gates for
852 murine rotavirus infection were set based on naïve samples.

853 Where indicated, dissociated cells were enriched using MojoSort Mouse anti-APC
854 Nanobeads (BioLegend, #480072) after flow cytometry staining for anti-EpCAM and anti-CD45
855 with APC fluorophores by following manufacturer protocols.

856 **RNA sequencing and expression analysis**

857 Wild-type C57BL/6J or *Ifnlr1*$^{-/-}$ mice were administered *ad libitum* Kool-aid or ABX for two
858 weeks, or wild-type mice were administered 25μg recombinant IFN-λ for one day, then ileal
859 segments lacking Peyer's patches were harvested and RNA sequencing was performed as prior
860 (Park et al., 2016). mRNA from ilea was purified with oligo-dT beads (Invitrogen, Carlsbad, CA)
861 and cDNA was synthesized using a custom oligo-dT primer containing a barcode and adaptor-
862 linker sequence, degradation of RNA-DNA hybrid following single-strand synthesis, and ligation
863 of a second sequencing linker with T4 ligase (New England Biolabs, Ipswich, MA). These
864 reactions were cleaned up by solid phase reversible immobilization (SPRI), followed by
865 enrichment by PCR and further SPRI to yield strand-specific RNA-seq libraries. Libraries were
866 sequenced with an Illumina HiSeq 2500 with three to four mice were included in each group.
867 Samples were demultiplexed with second mate, reads were aligned with STAR aligner and then
868 counted with HT-Seq. Differentially expressed genes were identified using DESeq2 (Love et al.,
869 2014) based on cutoffs of 2-fold change, and an inclusive p-value < 0.5. Standard gene set
870 enrichment analysis was performed to identify enrichments in IFN-λ response genes. RNA-seq
871 data were uploaded to the European Nucleotide Archive (accession #: PRJEB43446).

872 **16S rRNA gene Illumina sequencing and analysis**

873 For sequencing of the 16S rRNA gene, primer selection and PCRs were performed as
874 described previously (Caporaso et al., 2011). Briefly, each sample was amplified in triplicate with
875 Golay-barcoded primers specific for the V4 region (F515/R806), combined, and confirmed by gel
876 electrophoresis. PCR reactions contained 18.8μL RNase/DNase-free water, 2.5μL of 10X High
877 Fidelity PCR Buffer (Invitrogen, 11304-102), 0.5μL of 10 mM dNTPs, 1μL 50 of mM MgSO4, 0.5μL
878 each of forward and reverse primers (10 μM final concentration), 0.1μL of Platinum High Fidelity

879 Taq (Invitrogen, 11304-102), and 1.0μL genomic DNA. Reactions were held at 94°C for 2 min to
880 denature the DNA, with amplification proceeding for 26 cycles at 94°C for 15 s, 50°C for 30 s, and
881 68°C for 30 s; a final extension of 2 min at 68°C was added to ensure complete amplification.
882 Amplicons were pooled and purified with 0.6x Agencourt AMPure XP beads (Beckman-Coulter,
883 A63882) according to the manufacturer's instructions. The final pooled samples, along with
884 aliquots of the three sequencing primers, were sent to the DNA Sequencing Innovation Lab
885 (Washington University School of Medicine) for sequencing by the 2 X 250bp protocol with the
886 Illumina MiSeq platform.

887 Read quality control and the resolution of amplicon sequence variants were performed in
888 R with DADA2 (Callahan et al., 2016). Non-bacterial amplicon sequence variants were filtered
889 out. The remaining reads were assigned taxonomy using the Ribosomal Database Project (RDP
890 trainset 16/release 11.5) 16S rRNA gene sequence database (Cole et al., 2014). Ecological
891 analyses, such as alpha-diversity (richness, Shannon diversity) and beta-diversity analyses
892 (UniFrac distances), were performed using PhyloSeq and additional R packages (McMurdie and
893 Holmes, 2013). 16S sequencing data have been uploaded to the European Nucleotide Archive
894 (accession #: PRJEB43446).

895 **Single-cell RNA Sequencing Analyses**

896 A mouse single-cell RNA sequencing dataset generated by Haber et al. was accessed
897 from NCBI's Gene Expression Omnibus (GEO), accession #: GSE92332. A human pediatric
898 single-cell RNA sequencing dataset generated by Elmentaite et al. was accessed in processed
899 form from The Gut Cell Atlas, with raw data also available on EMBL-EBI Array Express, accession
900 #: E-MTAB-8901. Files were analyzed in R using Seurat (v. 3.2.2) (Stuart and Butler et al., 2019).
901 For the Haber et al. dataset, UMI counts were normalized to counts per million, log2 transformed,
902 and homeostatic ISGs were selected for analysis. Data was collated by previously annotated cell-
903 type and proportion of cells expressing each individual ISG was calculated. For Elmentaite et al,

904 data was restricted to healthy controls and then collated by previously annotated cell-type to
905 determine the proportion of cells expressing individual ISGs.

906 **Statistical Analyses**

907 Sample size estimation was performed based on historical data. Data were analyzed with
908 Prism software (GraphPad Prism Software), with specified tests as noted in the figure legends.

909 **Data availability.**

910 RNA sequencing data obtained in this study have been deposited in the European
911 Nucleotide Archive (accession #: PRJEB43446).

912

913 **Acknowledgments**

914 The authors would like to thank the following OHSU core facilities: Integrated Genomics
915 Laboratory, Advanced Light Microscopy Core, and Histopathology Core; and the following
916 WUSTL core facilities: Genome Technology Access Center. T.J.N. was supported NIH grant R01-
917 AI130055 and by a faculty development award from the Sunlin & Priscilla Chou Foundation. J.A.V.
918 was supported by NIH grants T32-GM071338 and T32-AI007472. M.T.B. was supported by NIH
919 grants R01-AI139314, R01-AI141716, and R01-AI141478, the Pew Biomedical Scholars Program
920 of the Pew Charitable Trusts, and a Children's Discovery Institute of Washington University and
921 St. Louis Children's Hospital Interdisciplinary Research Initiative grant (MI-II-2019–790). The
922 funders had no role in study design, data collection and interpretation, or the decision to submit
923 the work for publication.

924

925 **Author Contributions**

926 Conceptualization, J.A.V., M.T.B., and T.J.N.; Methodology, J.A.V., M.T.B., and T.J.N.;
927 Investigation, J.A.V., S.T.P., E.A.K., M.W., H.I., R.R., C.D., D.C., A.W., M.A., S.L., and T.J.N.;
928 Writing – Original Draft, J.A.V.; Writing – Review & Editing, J.A.V., M.T.B., and T.J.N.;

Visualization, J.A.V.; Supervision, M.T.B. and T.J.N.; Project Administration, L.L., M.T.B., and T.J.N.; Funding Acquisition, M.T.B. and T.J.N.

Disclosure

We declare no competing interests.

934 **References**

935 Abt, M.C., Osborne, L.C., Monticelli, L.A., Doering, T.A., Alenghat, T., Sonnenberg, G.F., Paley,
936 M.A., Antenus, M., Williams, K.L., Erikson, J., et al. (2012). Commensal bacteria calibrate the
937 activation threshold of innate antiviral immunity. Immunity *37*, 158–170.

938 Arnold, M.M., Sen, A., Greenberg, H.B., and Patton, J.T. (2013). The battle between rotavirus
939 and its host for control of the interferon signaling pathway. PLoS Pathog. *9*, e1003064.

940 Atuma, C., Strugala, V., Allen, A., and Holm, L. (2001). The adherent gastrointestinal mucus gel
941 layer: thickness and physical state in vivo. Am. J. Physiol. Gastrointest. Liver Physiol. *280*,
942 G922-9.

943 Baldridge, M.T., Nice, T.J., McCune, B.T., Yokoyama, C.C., Kambal, A., Wheadon, M.,
944 Diamond, M.S., Ivanova, Y., Artyomov, M., and Virgin, H.W. (2015). Commensal microbes and
945 interferon-λ determine persistence of enteric murine norovirus infection. Science *347*, 266–269.

946 Baldridge, M.T., Lee, S., Brown, J.J., McAllister, N., Urbanek, K., Dermody, T.S., Nice, T.J., and
947 Virgin, H.W. (2017). Expression of Ifnlr1 on Intestinal Epithelial Cells Is Critical to the Antiviral
948 Effects of Interferon Lambda against Norovirus and Reovirus. J. Virol. *91*, JVI.02079-16.

949 Bradley, K.C., Finsterbusch, K., Schnepf, D., Crotta, S., Llorian, M., Davidson, S., Fuchs, S.Y.,
950 Staeheli, P., and Wack, A. (2019). Microbiota-Driven Tonic Interferon Signals in Lung Stromal
951 Cells Protect from Influenza Virus Infection. Cell Rep. *28*, 245-256.e4.

952 Burns, J.W., Krishnaney, A.A., Vo, P.T., Rouse, R. V., Anderson, L.J., and Greenberg, H.B.
953 (1995). Analyses of homologous rotavirus infection in the mouse model. Virology *207*, 143–153.

954 Callahan, B.J., McMurdie, P.J., Rosen, M.J., Han, A.W., Johnson, A.J.A., and Holmes, S.P.
955 (2016). DADA2: High-resolution sample inference from Illumina amplicon data. Nat. Methods
956 *13*, 581–583.

957 Caporaso, J.G., Lauber, C.L., Walters, W.A., Berg-Lyons, D., Lozupone, C.A., Turnbaugh, P.J.,
958 Fierer, N., and Knight, R. (2011). Global patterns of 16S rRNA diversity at a depth of millions of
959 sequences per sample. Proc. Natl. Acad. Sci. *108*, 4516–4522.

960 Chieppa, M., Rescigno, M., Huang, A.Y.C., and Germain, R.N. (2006). Dynamic imaging of
961 dendritic cell extension into the small bowel lumen in response to epithelial cell TLR
962 engagement. J. Exp. Med. *203*, 2841–2852.

963 Chu, H., and Mazmanian, S.K. (2013). Innate immune recognition of the microbiota promotes
964 host-microbial symbiosis. Nat. Immunol. *14*, 668–675.

965 Cole, J.R., Wang, Q., Fish, J.A., Chai, B., McGarrell, D.M., Sun, Y., Brown, C.T., Porras-Alfaro,
966 A., Kuske, C.R., and Tiedje, J.M. (2014). Ribosomal Database Project: data and tools for high
967 throughput rRNA analysis. Nucleic Acids Res. *42*, D633-42.

968 Elmentaite, R., Ross, A.D.B., Roberts, K., James, K.R., Ortmann, D., Gomes, T., Nayak, K.,
969 Tuck, L., Pritchard, S., Bayraktar, O.A., et al. (2020). Single-Cell Sequencing of Developing
970 Human Gut Reveals Transcriptional Links to Childhood Crohn's Disease. Dev. Cell *55*, 771-
971 783.e5.

972 Fenaux, M., Cuadras, M.A., Feng, N., Jaimes, M., and Greenberg, H.B. (2006). Extraintestinal
973 spread and replication of a homologous EC rotavirus strain and a heterologous rhesus rotavirus
974 in BALB/c mice. J. Virol. *80*, 5219–5232.

975 Ganal, S.C., Sanos, S.L., Kallfass, C., Oberle, K., Johner, C., Kirschning, C., Lienenklaus, S.,
976 Weiss, S., Staeheli, P., Aichele, P., et al. (2012). Priming of natural killer cells by nonmucosal
977 mononuclear phagocytes requires instructive signals from commensal microbiota. Immunity *37*,

171–186.

Haber, A.L., Biton, M., Rogel, N., Herbst, R.H., Shekhar, K., Smillie, C., Burgin, G., Delorey, T.M., Howitt, M.R., Katz, Y., et al. (2017). A single-cell survey of the small intestinal epithelium. Nature *551*, 333–339.

Hakim, M.S., Chen, S., Ding, S., Yin, Y., Ikram, A., Ma, X.X., Wang, W., Peppelenbosch, M.P., and Pan, Q. (2018). Basal interferon signaling and therapeutic use of interferons in controlling rotavirus infection in human intestinal cells and organoids. Sci. Rep. *8*, 1–13.

Hernández, P.P., Mahlakoiv, T., Yang, I., Schwierzeck, V., Guendel, F., Gronke, K., Ryffel, B., Dumoutier, L., Renauld, J., and Suerbaum, S. (2015). Interferon-λ and interleukin-22 cooperate for the induction of interferon-stimulated genes and control of rotavirus infection. Nat. Immunol. *16*, 698–707.

Honda, K., and Littman, D.R. (2016). The microbiota in adaptive immune homeostasis and disease. Nature *535*, 75–84.

Honda, K., Yanai, H., Negishi, H., Asagiri, M., Sato, M., Mizutani, T., Shimada, N., Ohba, Y., Takaoka, A., Yoshida, N., et al. (2005a). IRF-7 is the master regulator of type-I interferon-dependent immune responses. Nature *434*, 772–777.

Honda, K., Ohba, Y., Yanai, H., Negishi, H., Mizutani, T., Takaoka, A., Taya, C., and Taniguchi, T. (2005b). Spatiotemporal regulation of MyD88-IRF-7 signalling for robust type-I interferon induction. Nature *434*, 1035–1040.

Ingle, H., Peterson, S.T., and Baldridge, M.T. (2018). Distinct Effects of Type I and III Interferons on Enteric Viruses. Viruses *10*.

Ingle, H., Hassan, E., Gawron, J., Mihi, B., Li, Y., Kennedy, E.A., Kalugotla, G., Makimaa, H., Lee, S., Desai, P., et al. (2021). Murine astrovirus tropism for goblet cells and enterocytes facilitates an IFN-λ response in vivo and in enteroid cultures. Mucosal Immunol. *14*, 751–761.

Iwasaki, A., and Medzhitov, R. (2015). Control of adaptive immunity by the innate immune system. Nat. Immunol. *16*, 343–353.

Johansson, M.E. V., Larsson, J.M.H., and Hansson, G.C. (2011). The two mucus layers of colon are organized by the MUC2 mucin, whereas the outer layer is a legislator of host-microbial interactions. Proc. Natl. Acad. Sci. *108*, 4659–4665.

Kim, S., Covington, A., and Pamer, E.G. (2017). The intestinal microbiota: Antibiotics, colonization resistance, and enteric pathogens. Immunol. Rev. *279*, 90–105.

Kotenko, S. V, and Durbin, J.E. (2017). Contribution of type III interferons to antiviral immunity: Location, Location, Location. J. Biol. Chem. *292*, 7295–7303.

Krajmalnik-Brown, R., Ilhan, Z.E., Kang, D.W., and DiBaise, J.K. (2012). Effects of gut microbes on nutrient absorption and energy regulation. Nutr. Clin. Pract. *27*, 201–214.

Levy, D.E., and García-Sastre, A. (2001). The virus battles: IFN induction of the antiviral state and mechanisms of viral evasion. Cytokine Growth Factor Rev. *12*, 143–156.

Liberzon, A., Birger, C., Thorvaldsdóttir, H., Ghandi, M., Mesirov, J.P., and Tamayo, P. (2016). The Molecular Signatures Database (MSigDB) hallmark gene set collection. Cell Syst. *1*, 417–425.

Lin, J.-D., Feng, N., Sen, A., Balan, M., Tseng, H.-C., McElrath, C., Smirnov, S. V., Peng, J., Yasukawa, L.L., Durbin, R.K., et al. (2016). Distinct Roles of Type I and Type III Interferons in Intestinal Immunity to Homologous and Heterologous Rotavirus Infections. PLoS Pathog. *12*, e1005600.

1022 Love, M.I., Huber, W., and Anders, S. (2014). Moderated estimation of fold change and
1023 dispersion for RNA-seq data with DESeq2. Genome Biol. *15*, 550.

1024 Mahlakõiv, T., Hernandez, P., Gronke, K., Diefenbach, A., and Staeheli, P. (2015). Leukocyte-
1025 derived IFN-α/β and epithelial IFN-λ constitute a compartmentalized mucosal defense system
1026 that restricts enteric virus infections. PLoS Pathog. *11*, e1004782.

1027 McDole, J.R., Wheeler, L.W., McDonald, K.G., Wang, B., Konjufca, V., Knoop, K.A., Newberry,
1028 R.D., and Miller, M.J. (2012). Goblet cells deliver luminal antigen to CD103 + dendritic cells in
1029 the small intestine. Nature *483*, 345–349.

1030 McMurdie, P.J., and Holmes, S. (2013). phyloseq: an R package for reproducible interactive
1031 analysis and graphics of microbiome census data. PLoS One *8*, e61217.

1032 Monroe, K.M., McWhirter, S.M., and Vance, R.E. (2010). Induction of type I interferons by
1033 bacteria. Cell. Microbiol. *12*, 881–890.

1034 Nadkarni, M., Martin, F.E., Jacques, N.A., and Hunter, N. (2002). Determination of bacterial load
1035 by real-time PCR using a broad range (universal) probe and primer set. Microbiology *148*, 257–
1036 266.

1037 Nice, T.J., Baldridge, M.T., McCune, B.T., Norman, J.M., Lazear, H.M., Artyomov, M., Diamond,
1038 M.S., and Virgin, H.W. (2015). Interferon-λ cures persistent murine norovirus infection in the
1039 absence of adaptive immunity. Science *347*, 269–273.

1040 Nice, T.J., Osborne, L.C., Tomov, V.T., Artis, D., Wherry, E.J.J., and Virgin, H.W. (2016). Type I
1041 Interferon Receptor Deficiency in Dendritic Cells Facilitates Systemic Murine Norovirus
1042 Persistence Despite Enhanced Adaptive Immunity. PLoS Pathog. *12*, e1005684.

1043 Niess, J.H., Brand, S., Gu, X., Landsman, L., Jung, S., McCormick, B.A., Vyas, J.M., Boes, M.,
1044 Ploegh, H.L., Fox, J.G., et al. (2005). CX3CR1-mediated dendritic cell access to the intestinal
1045 lumen and bacterial clearance. Science *307*, 254–258.

1046 Odendall, C., Voak, A.A., and Kagan, J.C. (2017). Type III IFNs Are Commonly Induced by
1047 Bacteria-Sensing TLRs and Reinforce Epithelial Barriers during Infection. J. Immunol. *199*,
1048 3270–3279.

1049 Osterlund, P.I., Pietilä, T.E., Veckman, V., Kotenko, S. V, and Julkunen, I. (2007). IFN
1050 regulatory factor family members differentially regulate the expression of type III IFN (IFN-
1051 lambda) genes. J. Immunol. *179*, 3434–3442.

1052 Park, S., Buck, M.D., Desai, C., Zhang, X., Loginicheva, E., Martinez, J., Freeman, M.L., Saitoh,
1053 T., Akira, S., Guan, J.L., et al. (2016). Autophagy Genes Enhance Murine Gammaherpesvirus
1054 68 Reactivation from Latency by Preventing Virus-Induced Systemic Inflammation. Cell Host
1055 Microbe *19*, 91–101.

1056 Pott, J., Mahlakoiv, T., Mordstein, M., Duerr, C.U., Michiels, T., Stockinger, S., Staeheli, P., and
1057 Hornef, M.W. (2011). IFN-λ determines the intestinal epithelial antiviral host defense. Proc. Natl.
1058 Acad. Sci. *108*, 7944–7949.

1059 Rojas, J.M., Alejo, A., Martín, V., and Sevilla, N. (2021). Viral pathogen-induced mechanisms to
1060 antagonize mammalian interferon (IFN) signaling pathway. Cell. Mol. Life Sci. *78*, 1423–1444.

1061 Rooks, M.G., and Garrett, W.S. (2016). Gut microbiota, metabolites and host immunity. Nat.
1062 Rev. Immunol. *16*, 341–352.

1063 Sadler, A.J., and Williams, B.R.G. (2008). Interferon-inducible antiviral effectors. Nat. Rev.
1064 Immunol. *8*, 559–568.

1065 Schmid, S., Mordstein, M., Kochs, G., García-Sastre, A., and TenOever, B.R. (2010).

1066 Transcription factor redundancy ensures induction of the antiviral state. J. Biol. Chem. *285*,
1067 42013–42022.

1068 Schneider, W.M., Chevillotte, M.D., and Rice, C.M. (2014). Interferon-stimulated genes: a
1069 complex web of host defenses. Annu. Rev. Immunol. *32*, 513–545.

1070 Schoggins, J.W., and Rice, C.M. (2011). Interferon-stimulated genes and their antiviral effector
1071 functions. Curr. Opin. Virol. *1*, 519–525.

1072 Shi, Z., Zou, J., Zhang, Z., Zhao, X., Noriega, J., Zhang, B., Zhao, C., Ingle, H., Bittinger, K.,
1073 Mattei, L.M., et al. (2019). Segmented Filamentous Bacteria Prevent and Cure Rotavirus
1074 Infection. Cell *179*, 644-658.e13.

1075 Sommereyns, C., Paul, S., Staeheli, P., and Michiels, T. (2008). IFN-Lambda (IFN-λ) Is
1076 Expressed in a Tissue-Dependent Fashion and Primarily Acts on Epithelial Cells In Vivo. PLoS
1077 Pathog. *4*, e1000017.

1078 Steed, A.L., Christophi, G.P., Kaiko, G.E., Sun, L., Goodwin, V.M., Jain, U., Esaulova, E.,
1079 Artyomov, M.N., Morales, D.J., Holtzman, M.J., et al. (2017). The microbial metabolite
1080 desaminotyrosine protects from influenza through type I interferon. Science (80-.). *357*, 498–
1081 502.

1082 Stefan, K.L., Kim, M. V, Iwasaki, A., and Kasper, D.L. (2020). Commensal Microbiota
1083 Modulation of Natural Resistance to Virus Infection. Cell *183*, 1312-1324.e10.

1084 Stockinger, S., Duerr, C.U., Fulde, M., Dolowschiak, T., Pott, J., Yang, I., Eibach, D., Bäckhed,
1085 F., Akira, S., Suerbaum, S., et al. (2014). TRIF signaling drives homeostatic intestinal epithelial
1086 antimicrobial peptide expression. J. Immunol. *193*, 4223–4234.

1087 Stuart, T., Butler, A., Hoffman, P., Hafemeister, C., Papalexi, E., Mauck, W.M., Hao, Y.,
1088 Stoeckius, M., Smibert, P., and Satija, R. (2019). Comprehensive Integration of Single-Cell
1089 Data. Cell *177*, 1888-1902.e21.

1090 Swamy, M., Abeler-Dörner, L., Chettle, J., Mahlakõiv, T., Goubau, D., Chakravarty, P., Ramsay,
1091 G., Reis e Sousa, C., Staeheli, P., Blacklaws, B.A., et al. (2015). Intestinal intraepithelial
1092 lymphocyte activation promotes innate antiviral resistance. Nat. Commun. *6*, 7090.

1093 Taylor, K.E., and Mossman, K.L. (2013). Recent advances in understanding viral evasion of
1094 type I interferon. Immunology *138*, 190–197.

1095 Thompson, M.R., Kaminski, J.J., Kurt-Jones, E.A., and Fitzgerald, K.A. (2011). Pattern
1096 recognition receptors and the innate immune response to viral infection. Viruses *3*, 920–940.

1097 Tomasello, E., Naciri, K., Chelbi, R., Bessou, G., Fries, A., Gressier, E., Abbas, A., Pollet, E.,
1098 Pierre, P., Lawrence, T., et al. (2018). Molecular dissection of plasmacytoid dendritic cell
1099 activation in vivo during a viral infection. EMBO J. *37*, 1–19.

1100 Uchiyama, R., Chassaing, B., Zhang, B., and Gewirtz, A.T. (2014). Antibiotic treatment
1101 suppresses rotavirus infection and enhances specific humoral immunity. J. Infect. Dis. *210*,
1102 171–182.

1103 Williams, J.M., Duckworth, C.A., Burkitt, M.D., Watson, A.J.M., Campbell, B.J., and Pritchard,
1104 D.M. (2015). Epithelial cell shedding and barrier function: a matter of life and death at the small
1105 intestinal villus tip. Vet. Pathol. *52*, 445–455.

1106 Van Winkle, J.A., Constant, D.A., Li, L., and Nice, T.J. (2020). Selective Interferon Responses
1107 of Intestinal Epithelial Cells Minimize Tumor Necrosis Factor Alpha Cytotoxicity. J. Virol. *94*,
1108 e00603-20.

1109 Winkler, E.S., Shrihari, S., Hykes, B.L., Handley, S.A., Andhey, P.S., Huang, Y.-J.S., Swain, A.,

1110 Droit, L., Chebrolu, K.K., Mack, M., et al. (2020). The Intestinal Microbiome Restricts Alphavirus
1111 Infection and Dissemination through a Bile Acid-Type I IFN Signaling Axis. Cell *182*, 901-
1112 918.e18.

1113 Zhang, B., Chassaing, B., Shi, Z., Uchiyama, R., Zhang, Z., Denning, T.L., Crawford, S.E.,
1114 Pruijssers, A.J., Iskarpatyoti, J.A., Estes, M.K., et al. (2014). Viral infection. Prevention and cure
1115 of rotavirus infection via TLR5/NLRC4-mediated production of IL-22 and IL-18. Science (80-.).
1116 *346*, 861–865.

1117